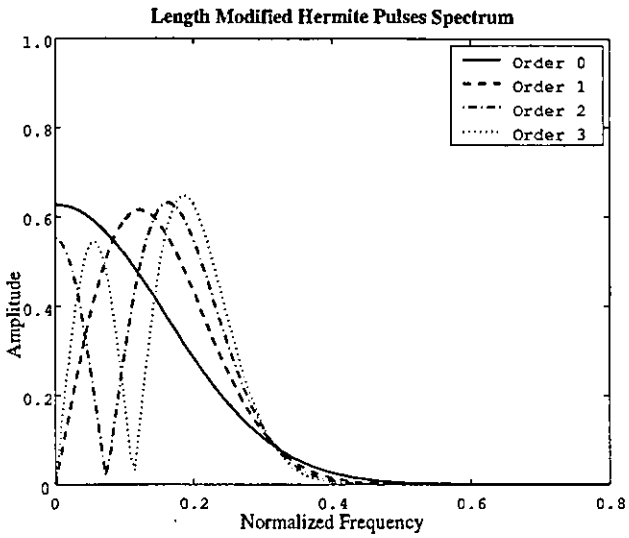

Fig. 2. Spectrum of the modified Hermite pulses, for orders from 0 to 3. All of them are limited to the same frequency.

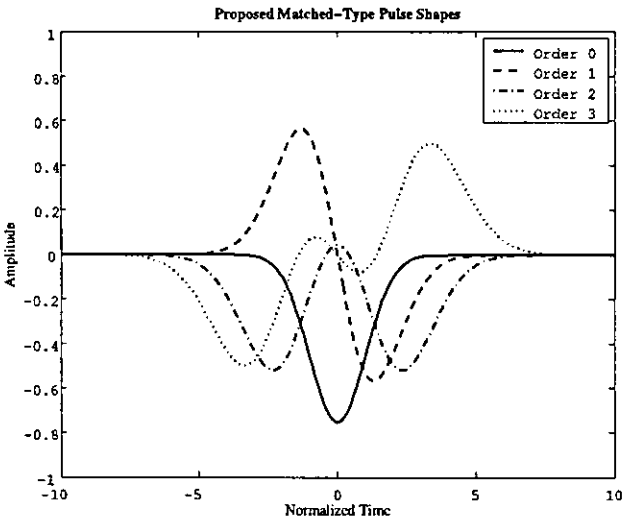

Fig. 3. Proposed Matched type pulse shapes for orders from 0 to 3.

This is because when $m = n$, the two pulses in (13) are the original Hermite pulses equally scaled, and hence orthogonal. For the case of Non-Matched receiver, the values of the matrix in (12) are given by the correlation between the upper-frequency limited Hermite pulses and the original Hermite pulses described by (1), resulting in

$$c^N_{n,m} = \int_{-\infty}^{\infty} \varphi_n(t, \alpha_n)\psi_m(t)dt, \tag{14}$$

where N means Non Matched, and as before $m, n \in \{0, ..., N-1\}$. In this case, the matrix elements in (12) differ from unity, except for the case of $\alpha_n = 1$, when the modified pulse described by (5) equals the original Hermite pulses described by (1). Assuming that $\mathbf{C}$ has full rank, it can be decomposed into an orthogonal matrix $\mathbf{Q}$ and an upper triangular matrix $\mathbf{R}$ as follows

$$\mathbf{C} = \mathbf{Q}.\mathbf{R}. \tag{15}$$

Defining $\mathbf{X}$ as the inverse matrix of $\mathbf{R}$, we have

$$\mathbf{Q} = \mathbf{C}\mathbf{X}. \tag{16}$$

As defined above, $\mathbf{C}$ represents the pseudo-channel between the transmitter and receiver. If the columns of $\mathbf{X}$ represent the N symbols of the used transmit alphabet, then the columns of $\mathbf{Q}$ represent the received signals just before the bank of correlators, these columns are mutually orthogonal, which was the objective of this section.

C. The transmit signal

In this section, we describe the composition of the transmit signal determined by the columns of the matrix $\mathbf{X}$ defined in (16). For the Matched receiver case, we define the transmit pulses as the upper-frequency limited Hermite pulses defined in (5), with elements of $\mathbf{X}$ as coefficients, such that

$$\xi_m(t) = \eta^M_m \sum_{n=0}^{N-1} x_{n,m}\varphi_n(t, \alpha_n), \tag{17}$$

where, M stands for Matched and $x_{n,m}$ is the nth element in the mth column of $\mathbf{X}$. The normalization factor, η^M_m, can be found from equation (18).

$$(\eta^M_n)^2 \int_{-\infty}^{\infty} \sum_{n=0}^{N-1} \xi_n(t)^2 dt = 1 \tag{18}$$

An example of the proposed matched type pulses and their spectrum are shown in Figs. 3 and 4 respectively. For the Non-Matched receiver, the proposed transmit pulses are defined as the original Hermite pulses, defined in (1), having the elements of $\mathbf{X}$ as coefficients, such that

$$\zeta_m(t) = \eta^{NM}_m \sum_{n=0}^{N-1} x_{n,m}\psi_n(t), \tag{19}$$

where NM stands for Non-Matched and as before, $x_{n,m}$ is the nth element in the mth column of $\mathbf{X}$, and the normalization factor η^{NM}_m is derived from

$$(\eta^{NM}_n)^2 \int_{-\infty}^{\infty} \sum_{n=0}^{N-1} \zeta_n(t)^2 dt = 1. \tag{20}$$

An example of Non-Matched receiver proposed pulse shapes and their spectrum are illustrated in Figs. 5 and 6 respectively.

D. The receive template

For the Matched receiver type, similarly to the case of the transmit pulses composition, the templates are a combination of the upper-frequency limited Hermites pulses defined in (5)

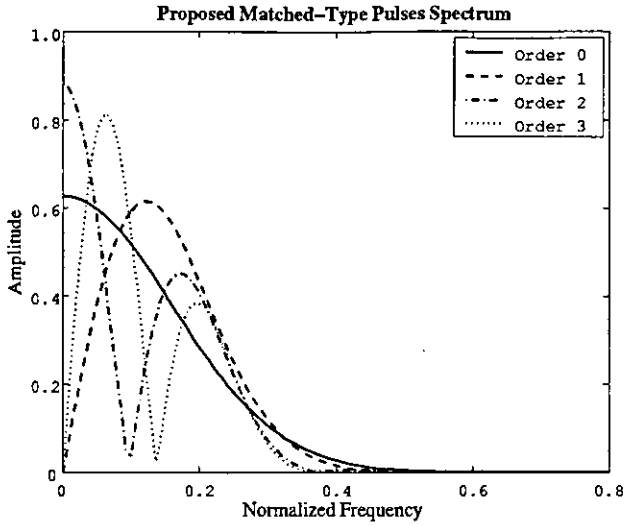

Fig. 4. Spectrum of the proposed Matched type pulse shapes for orders from 0 to 3.

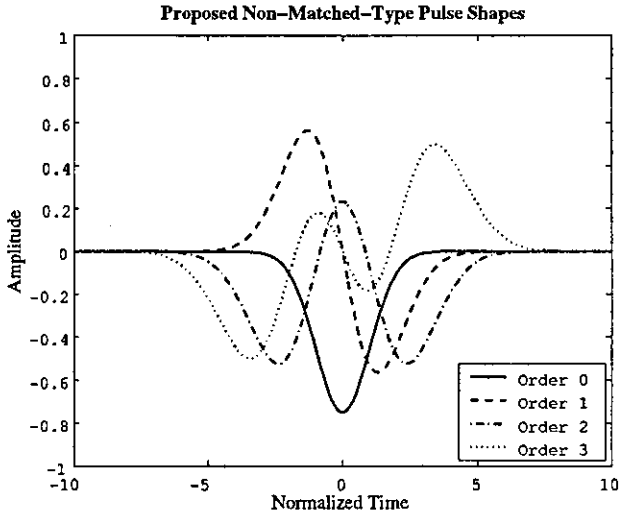

Fig. 5. Proposed Non-Matched type pulse shapes for orders from 0 to 3.

with the elements of the orthogonal matrix $\mathbf{Q}$ as coefficients. Then, these signals are given by

$$\vartheta_m^M(t) = \mu_m^M \sum_{n=0}^{N-1} q_{n,m}\varphi_n(t,\alpha_n), \tag{21}$$

where μ_m^M is a normalization coefficient defined by

$$\mu_m^M = \sqrt{\sum_{n=0}^{N-1} q_{n,m}^2}. \tag{22}$$

In case of the Non-Matched receiver, the receive template is the result of combining the original Hermite pulses, defined

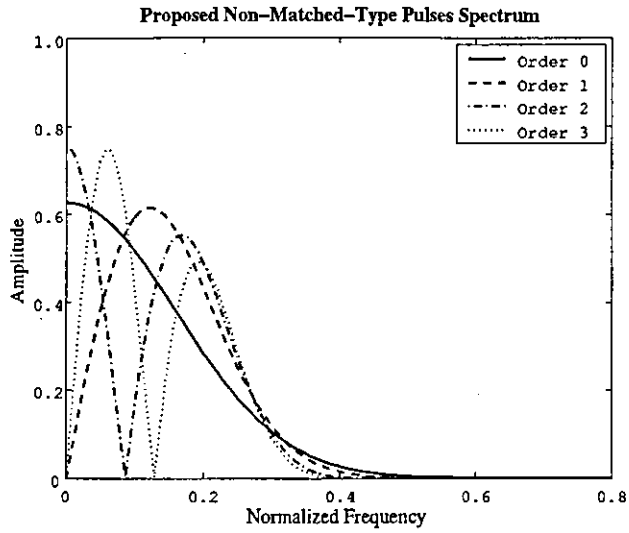

Fig. 6. Spectrum of the Proposed Non-Matched type pulse shapes for orders from 0 to 3.

in (1), with the elements of $\mathbf{Q}$ as coefficients, such that

$$\vartheta_m^{NM}(t) = \mu_m^{NM} \sum_{n=0}^{N-1} q_{n,m}\psi_n(t), \tag{23}$$

here, the normalization coefficient is defined by

$$\mu_m^{NM} = \sqrt{\sum_{n=0}^{N-1} q_{n,m}^2}. \tag{24}$$

IV. Performance Evaluation

In this section, we evaluate the performance of the two proposed set of pulses against the original set of Hermite pulses. The original Hermite pulses are scaled with a common width modifying factor which allows two conditions: first, the minimum order of the set of used pulses has its upper frequency limit set to the desired frequency, and second, the set of Hermite pulses remain mutually orthogonal because the introduced scaling factor is the same for all the set in the alphabet. We are going to assume a 4-ary system, and a limit frequency $fc = 0.29$ in the normalized frequency scale. The width scaling factor for the original Hermite pulses is the one corresponding to the degree zero, $\alpha_0 = 1$; the other factors are $\alpha_1 = 0.7650$, $\alpha_2 = 0.6485$ and $\alpha_3 = 0.5746$. Fig. 7 shows the BER comparison between the two proposed sets of pulses and the original Hermite set of pulses. The conventional set of pulses outperforms the proposed pulses for an ideal non-limited frequency spectrum. And as expected, the Matched type proposed set of pulses presents better BER performance than the Non-Matched type, because, the receive templates are the same as the transmit signals, while in the Non-Matched type, the receive templates are the conventional Hermite pulses.

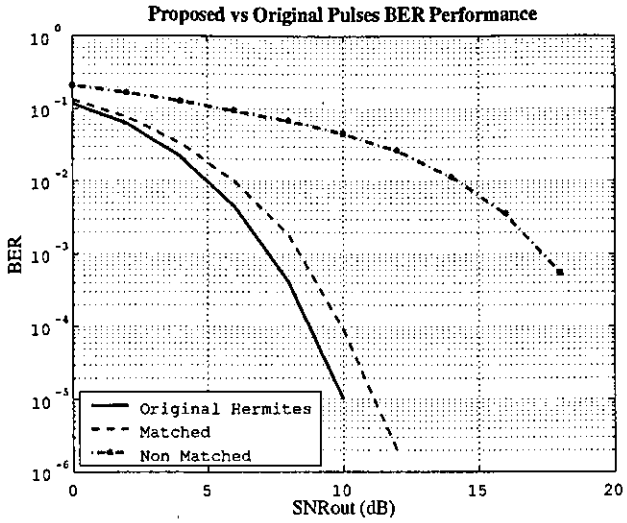

Fig. 7. BER comparison of the proposed pulses and the original Hermite pulses using a set of the 4 first order pulses.

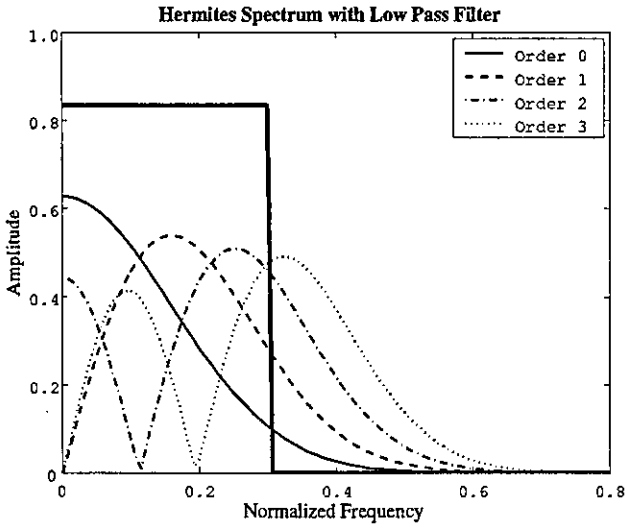

Fig. 8. Ideal restrictive filter applied to the Convention Hermite pulses.

A. *Low Frequency Band Restriction*

We are are going to assume the existence of a restriction in the frequency spectrum, which constrains the bandwidth of UWB systems to a low frequency band. Lets assume that such limitation demands the application of a filter which is ideally represented in Fig. 8, and is shown applied over the conventional Hermites frequency response plot. The bit error rate result of this restriction is shown in Fig. 9. Compared with the previous results shown in Fig. 7, we appreciate that the proposed sets of pulses perform better than the conventional Hermites. It is because of lose of orthogonality on the conventional Hermite set. Then, our proposed sets of pulses shows to be more robust for the study case presented in this section.

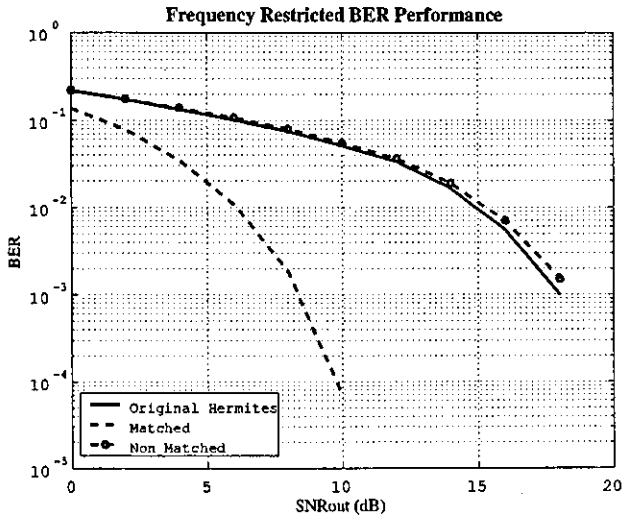

Fig. 9. BER of Conventional and proposed pulses with a low pass filter.

V. Conclusion

In this paper, we derived two sets of mutually orthogonal waveforms which have their upper frequency fixed by design to the same value. The difference between them depends on whether the receive templates are matched or non matched to the transmit pulse shapes. The proposed sets of pulses, particularly the Matched type, present better BER performance when employing a filter like in study case presented in the previous section.

References

[1] M. Ghavami, L. B. Michael and R. Kohno, "Hermite Function Based Orthogonal Pulses for Ultra Wideband Communications," *Proceedings of the WPMC'01 - Aalborg, Denmark*, pp. 437-440, 2001.

[2] M. Z. Win and R. A. Scholtz, "Ultra-wide widebandwith time-hoppiing spread-spectrum impulse radio for wireless multiple access communications," *IEEE Trans. Commun.*, vol. 48, no. 4, pp. 679-691, Apr. 2000.

[3] G. T. F. de Abreu, "Orthogonal Designs for Advanced Wireless Communications," *Ph.D. dissertation*, Yokohama National University, Yokohama, Japan, 2004.

[4] G. T. F. de Abreu, C. J. Mitchel and R. Kohno, "On the Design of Orthogonal-Shape Modulation for UWB Systems Using Hermite Pulses," *Journal of Communication and Networks, vol.05*, pp. 100-124, Dec. 2002.

[5] J. A. N. da Silva and M. L. R. de Campos, "Orthogonal Pulse Shape Modulation for Impulse Radio," *in Proc. IEEE International Telecommunications Symposium (ITS'02), Natal, Brasil*, pp. 911-921, Sept. 2002.

[6] B. Sklar, Digital Communications: Fundamentals and Applications (2nd Edition), Prentice Hall 2001.

[7] G. T. F. de Abreu and R. Kohno, "Design of Jitter-Robust Orthogonal Pulses for UWB Systems," *International Communication Conference - Wireless Communications Symposium* (Globecomm 2003), December 1^{st}-5^{th}, 2003.

Parameter Estimation of UWB-IR Signals using Array Antennas with Hermite-Hadamard Orthogonal Filters

Giuseppe Thadeu Freitas de Abreu
Centre for Wireless Communications, University of Oulu
Tutkijantie 2E, 90570-Oulu, Finland
E-mail: giuseppe@ee.oulu.fi

Takashi Uefuji and Ryuji Kohno
Yokohama National University
79-5 Hodogaya, Yokohama, Japan 240-850
E-mail: [ue,kohno]@kohnolab.dnj.ynu.ac.jp

Abstract— **Direction of arrival (DoA) and time difference of arrival (TDoA) estimation for ultra-wideband impulse radio (UWB-IR) systems utilizing Gaussian waveforms is discussed. It is shown that the utilization of different orthonormal Hermite filters across the elements of an array of receive antennas enables some of parameter estimation techniques known for conventional (narrow band) array antenna systems to be almost straightforwardly employed in UWB-IR systems. The structure of bearing vectors in such set-ups is easily modeled using our previous theoretical results on the correlation properties of Hermite wavelets, which can accurately describe Gaussian waveforms considered for UWB-IR systems. Orthogonal filters are used across the array in order to avoid residual correlation of non-signal components at the output of different antenna elements. A Hadamard construction over the set of orthonormal Hermites is proposed to increase the apparent aperture of the array towards each point in the operational spatial-temporal window, leading to enhanced estimation accuracy. The technique can be useful in the design equipment for space-time sounding of the UWB channel.**

Keywords— **Ultra-wideband systems, DoA estimation, ToA estimation, array antennas.**

I. Introduction

Orthogonal Hermite wavelets were first proposed for wireless communications in [1] and later considered for Ultra-Wideband Impulse Radio (UWB-IR) in [2]–[4]. Unlike alternative orthogonal waveforms proposed for UWB-IR [5], [6], Hermite wavelets are Gaussian and, as such, offer both a more realistic and mathematically tractable model to the accurate representation of waveforms obtained with low-complexity impulse generators [7]–[9].

So far, most published works on the application of orthogonal wavelets to wireless communications have focused on their use as *transmit* waveforms [1], [3]–[6], [10]–[13]. Unfortunately, the orthogonality of such signals is easily lost in the presence of multipath, antenna distortion, jitter, frequency selective propagation and non-synchronized multi-user activity. In addition to these technical difficulties, regulation-imposed limitations on the spectra of UWB signals can hold impractical the design of orthogonal UWB-IR waveforms. These issues explain the widespread preference for Gaussian waveforms and a general consensus around the use of waveform-independent modulation schemes in UWB-IR systems.

In this paper, we discuss the utilization of orthogonal Hermite wavelets not as transmit pulses, but as a signal processing tool at the receiver side. We dwell on the fact that Gaussian waveforms commonly considered for UWB-IR systems, can be accurately modeled by Hermite wavelets [7], [14]. Our approach is to exploit the properties of the correlation functions of such waveforms [13], [14], to extract directly from the UWB impulsive signal, similar conditions to those required by well-known parameter estimation techniques originally developed within the theory of narrowband (carrier-based) communications systems.

The remainder of the paper is as follows. In section II, we introduce the structure of the array receiver. In section III, comments on each component of the array covariance matrix and its impact on the parameter estimation problem are given. In section IV examples are given on how well-known algorithms develop for narrow-band signal processing can be employed in UWB systems. The corresponding simulation results are shown in section V and conclusions are drawn in section VI

II. Array Receiver Structure

Consider an arbitrary array of N antennas (sensors) immersed in an isotropic medium. For simplicity we will restrict ourselves to a two-dimensional space, since the extension to the general three-dimensional case is straightforward.

Let us denote the distance from the n-th to the 0-th element by d_n and, without loss of generality, label the antenna elements such that d_{N-1} is the largest dimension of the array. Assuming that the array is roughly synchronized to the impinging pulses, d_{N-1} must satisfy the following condition in order to ensure that all the elements receive the same pulse:

$$d_{N-1} \leqslant cT, \tag{1}$$

where c is the propagation speed in the medium and T is the duration of the impulsive waveform used in the system.

The product $\lambda = cT$ is in fact the length of the receive waveform (a single impulse) and is hereafter referred to as the *wavelength* of the signal. In light of this terminology, the condition given in equation (1) is equivalent to that commonly employed narrow-band array antenna theory, only that here, due to the impulsive (non-periodic) nature of the signals, the condition is imposed on the total array size, rather than the inter-element spacing.

We emphasize that equation (1) do not result in particularly unrealistic array sizes. For example, if it is assumed that $T = 250$ picoseconds (which is a rather small figure), it is found that d_{N-1} can go up to 7.5 cm.

For illustrative reasons and for the sake of coherence with the literature, it is assumed that the waveform generated at the transmitter is the Gaussian pulse and that UWB antennas, due to size constraints, radiate at frequencies significantly lower than their optimum operating band, which effectively turn them into differentiating devices [15]. It is also considered that the effect of free space path loss over UWB pulses results in the integration of the signals [16], such that the signal at the output of a receive antenna is proportional to its first derivative (also known as the monocycle)[1].

The receive waveform can be therefore be modeled by the first-order Hermite wavelet, which belong to the family of orthonormal Hermite wavelets defined by

$$\psi_n(t) \triangleq \frac{H_n(t)e^{\frac{-t^2}{2}}}{\sqrt{2^n n!\sqrt{\pi}}}, \tag{2}$$

where [17]

$$H_n(t) \triangleq (-1)^n e^{t^2} \frac{d^n}{dt^n} e^{-t^2} \quad n \in \mathbb{N}. \tag{3}$$

[1]These assumptions are not essential and can be relaxed by assuming any Gaussian waveform at the receiver. In this case, a more general definition of Hermite wavelet can be used to model the signal [14].

Assume that a number K of UWB pulses, respectively bearing the symbols s_k, impinge onto the array from the directions $\theta_{k=0,\ \cdots,\ K-1}$, measured from an arbitrary reference. Without loss of generality, let the 0-th element of the array be also the reference as to the time of arrival of the incoming signals. Then, the relative delay associated to the n-th element of the array is given by

$$\Delta\tau_{k,n} = d_n \cos(\theta_k). \tag{4}$$

Let the signal received at the n-th element be compared (correlated against) a certain template wavelet $\phi_n(t)$. The array output in the presence of the k-th signal is then

$$\mathbf{a}_k(\tau_k, \theta_k) = \tag{5}$$
$$[R_{0,1}(\tau_k)\ R_{1,1}(\tau_k + \Delta\tau_{k,1})\ \cdots\ R_{N-1,1}(\tau_k + \Delta\tau_{k,N-1})]^{\mathrm{T}},$$

where $R_{n,m}(\tau)$ is the correlation function of $\phi_n(t)$ and $\psi_m(t)$, τ_k is the TDoA of the k-th signal and $^{\mathrm{T}}$ denotes transpose.

Hereafter, we shall drop the variables τ_k and θ_k from the notation whenever convenient, without compromising clarity.

Given all the above, the array receive vector in the presence of all K signals, interference and noise, is given by

$$\mathbf{r} = \sum_{k=0}^{N-1} s_k \mathbf{a}_k + \mathbf{w} = \mathbf{A}\cdot\mathbf{s} + \mathbf{w}, \tag{6}$$

where the matrix of array manifolds $\mathbf{A}$, the symbol vector $\mathbf{s}$, and the noise vector $\mathbf{w}$ are all real-valued and respectively given by

$$\mathbf{A} = [\mathbf{a}_0\ \mathbf{a}_1\ \cdots\ \mathbf{a}_{K-1}] \tag{7}$$
$$\mathbf{s} = [s_0\ s_1\ \cdots\ s_{K-1}]^{\mathrm{T}} \tag{8}$$
$$\mathbf{w} = [w_0\ w_1\ \cdots\ w_{N-1}]^{\mathrm{T}}. \tag{9}$$

Note that $\mathbf{w}$ in fact models the contributions at the output of the correlators of noise and interfering signals captured by the wideband antenna, as well residual correlation values resulting from imperfections both on the model of the receive waveform itself and on the implementation of the filter templates.

The similarity between the structure of the array receive vector given in equation (6) and that found in conventional (narrowband) array signal processing literature [18]–[20] is evident.

III. Parameter Estimation Techniques and Scenarios

A. The Noise Covariance Matrix

High-resolution parameter estimation techniques of lower complexity (compared to maximum likelihood methods [19]) rely on the information obtained directly from the covariance matrix of the array output vector [18] (or on higher order momenta of similar structure [20]). It is known that these techniques are sensitive to correlation among the noise entries of the noise vector (less so with cumulant-based methods).

The central limit theorem ensures that w_n have Gaussian statistics [21]. In addition, a classic communication-theoretic results on the correlation receiver [22] establishes that, if the correlation filters used at different antenna elements are mutually orthonormal, w_n are mutually independent. Furthermore, since these correlators are essentially ultra-wide passband filters, it is fair to assume that the spectra of w_n are white. Finally, if the correlation filter templates $\phi_n(t)$ have same energy (which we normalize to the unity, without loss of generality), the variance of all processes w_n are the same. In summary, the utilization of a different orthonormal wavelet at each antenna element, as indicated in (5), implies that $\mathbf{w}$ can be modeled as a sample vector of real additive white Gaussian (AWG) randoms, independent and identically distributed (IID), each with zero mean and variance σ_w^2, such that

$$\mathbf{R}_w = E\left[\mathbf{w}\cdot\mathbf{w}^{\mathrm{T}}\right] = \sigma_w^2\mathbf{I}. \tag{10}$$

where $E[\,]$ denotes expectance and $\mathbf{I}$ is the identity matrix.

Given the discussions above, the covariance matrix of an array receiver with orthogonal Hermite correlators is given by

$$\mathbf{R} = E\left[\mathbf{r}\cdot\mathbf{r}^{\mathrm{T}}\right] = \mathbf{A}E\left[\mathbf{s}\cdot\mathbf{s}^{\mathrm{T}}\right]\mathbf{A}^{\mathrm{T}} + \sigma_w^2\mathbf{I} = \mathbf{A}\cdot\mathbf{R}_s\cdot\mathbf{A}^{\mathrm{T}} + \sigma_w^2\mathbf{I}. \tag{11}$$

B. The Array Manifold Matrix

A natural choice for the orthonormal template wavelets used at the array antenna elements are the Hermite wavelets, as defined in equation (2). We have shown in [13] that the closed form expression for the correlation function of any arbitrary pair (n, m) of Hermite wavelets can be written as [2]

$$R_{n,m}(\tau) = \int_{-\infty}^{\infty}\psi_n(t)\psi_m(t-\tau)dt \tag{12}$$
$$= \frac{(-1)^{2m+n}\tau^{n+m}\sqrt{n!m!}}{\sqrt{2^{n+m}}}e^{-\frac{\tau^2}{4}}\sum_{k=0}^{\lfloor(n,m)\rfloor}\frac{(-1)^k\tau^{-2k}\sqrt{4^k}}{(n-k)!(m-k)!k!},$$

where $\lfloor(n,m)\rfloor$ denotes the minimum between the pair (n,m).

Figure 1 shows a few plots of equation (12).

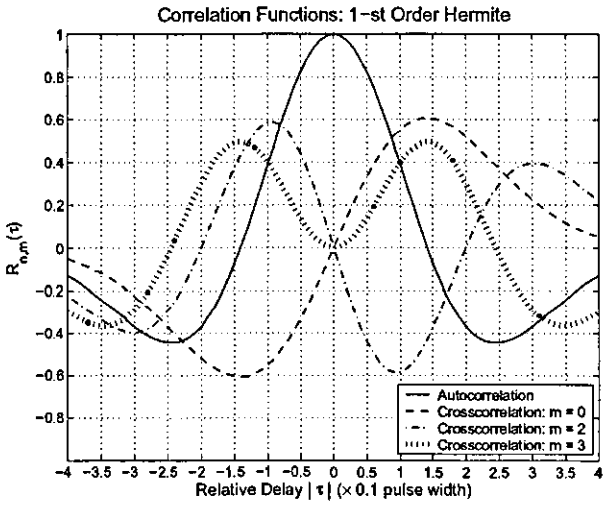

Fig. 1. Correlation functions of Hermite wavelets (Orders 0 to 3).

One problem that results from this choice of orthogonal filters, however, is that the output of the correlators which are not matched to the receive waveform can be negligible if $\tau_k + \Delta\tau_{k,1}$ are small.

Consider, for instance, that a Uniform Linear Array (ULA) is used and that a single UWB-IR source transmits from broadside, in perfect synchronism with the the RAKE finger in consideration at the receive array, such that $\theta + \Delta\theta = 0$. In this ideal case the array output vector is

$$\mathbf{a}_k(0,0) = [0\ 1\ 0\ \cdots\ 0]^{\mathrm{T}}. \tag{13}$$

This implies that the array would effectively responding as an omnidirectional antenna, which is a paradox given that the arrival of a impulse from broadside, at perfect synchronization with the filter bank, is the best possible scenario for reception!

C. Hermite-Hadamard Construction

The above problem can be solved by replacing the conventional Hermite templates with adequately designed waveforms that, while maintaining mutual orthogonality, return a truly collective output, that is, vectors with non-zero entries.

[2] A closed-form, unified expression of the correlation functions of generalized Hermite wavelets is given in [14], which can be used if the assumption on the waveform of received pulses is relaxed.

A systematic way to achieve this is to let the orthonormal template at the n-th element be the combination of M Hermite wavelets given below, where $b_{m,n}$ are real combining coefficients.

$$\phi_n(t) = \frac{1}{\sqrt{\beta}} \sum_{m=0}^{M-1} b_{n,m} \psi_n(t) \tag{14}$$

The array output is then given by

$$\mathbf{b}(\tau, \theta) = \mathbf{B} \cdot \mathbf{a}_M(\tau, \theta), \tag{15}$$

where the matrix of coefficients $\mathbf{B}$ is build from the entries $b_{n,m}$ and $\mathbf{a}_M(\tau, \theta)$ is as given in equation (5), only of length M.

In general, $\mathbf{B}$ must be computed so as to meet a given criterion (or minimize a certain cost function), subject to the preservation of its orthogonality. Mathematically we have

$$\min_{\mathbf{B}} f(\mathbf{B}) \quad \text{subject to} \quad \mathbf{B} \cdot \mathbf{B}^{\mathsf{T}} = \beta \mathbf{I} \quad (1 \leqslant \beta \leqslant M), \tag{16}$$

where β is referred to as the *weight* of $\mathbf{B}$ and $\mathbf{I}$ is the N-by-N identity matrix.

The constraint on $\mathbf{B}$ results from the fact that $\psi_n(t)$ are themselves orthonormal as well as the orthogonality condition on $\phi_n(t)$ and the limit on the Frobenius-norm (also known as the *energy*) of $\mathbf{B}$.

The above problem must be solved given the various conditioning parameters such as the set of distances d_n, the number of combined wavelets M and space-time window of interest. For example, assume that the array is to operate over a certain space-time interval Ω defined by

$$\Omega \triangleq \left\{ (\theta, \tau) \middle| \theta_{\min} \leqslant \theta \leqslant \theta_{\max},\ \tau_{\min} \leqslant \tau \leqslant \tau_{\max} \right\}. \tag{17}$$

If it is then required that the array gives the smoothest and largest possible output within Ω, one may define the cost function $f(\mathbf{B})$ as the normalized standard deviation

$$f(\mathbf{B}) = \frac{\sigma_\Omega}{\mu_\Omega}, \tag{18}$$

where μ_Ω and σ_Ω are the expected value of the norm of the output vector $\mathbf{b}$ and its standard deviation, respectively.

If all points in Ω are equally probable, Ω effectively defines an interval $[\bar{\tau}_{\min}, \bar{\tau}_{\max}]$, such that μ_Ω and σ_Ω^2 can be computed by

$$\mu_\Omega = \int_\Omega \left| \mathbf{a}(\tau)^{\mathsf{T}} \mathbf{B}^{\mathsf{T}} \mathbf{B} \mathbf{a}(\tau) \right| d\tau, \tag{19}$$

$$\sigma_\Omega^2 = \int_\Omega \left(\left| \mathbf{a}(\tau)^{\mathsf{T}} \mathbf{B}^{\mathsf{T}} \mathbf{B} \mathbf{a}(\tau) \right| - \mu_\Omega \right)^2 d\tau. \tag{20}$$

It is clear that an analytical solution of the above problem (even for particular cases) is extremely difficult. In fact, even numeric solutions may not be practical since an optimal coefficient matrix $\mathbf{B} \in \mathbb{R}^{N \times M}$ would be virtually impossible to implement.

A suboptimal (but feasible!) solution can be obtained if the entries of $\mathbf{B}$ are restricted to $\{-1, 0, 1\}$. The matrices with such a construction satisfying the condition in (16) are known in the mathematics literature as Weighing matrices [23], and contain the well-known Hadamard matrices as special cases. Even with this strong restriction, the solution of this problem is not trivial and is still under investigation by the authors.

In this paper, if only to gain insight, we take an ad-hoc approach and construct $\mathbf{B}$ by extracting N rows of the Hadamard matrix $\mathbf{H} \in \{1, -1\}^{M \times M}$, where $M = 2^{\lceil log_2 N \rceil}$ and $\lceil x \rceil$ denotes the smallest integer larger than x. Although none such matrices is optimal to all points in Ω, the matrix that maximizes the collective output of the array at any particular point in Ω is of such construction[3].

[3]This is because the partitions of permuted Hadamard matrices are all maximum weight Weighing matrices.

Defining the *apparent array size* as in equation (21), it is seen that this approach yields an upper-bound (envelope) to the largest achievable apparent array size with the particular array under consideration

$$\Sigma_N \triangleq |\mathbf{b}_N|. \tag{21}$$

Figure 2 compares the apparent sizes of arrays with 5 and 8 elements employing Hermite filters, against arrays with the same number of elements employing Hermite-Hadamard filters obtained from Hadamard matrices of size 8. The plots show that if pure orthonormal Hermite wavelets are employed, increasing the number of elements in the array does not result in a significant increase in the apparent array size, while better results are obtained if orthogonal Hadamard-Hermite filters are used.

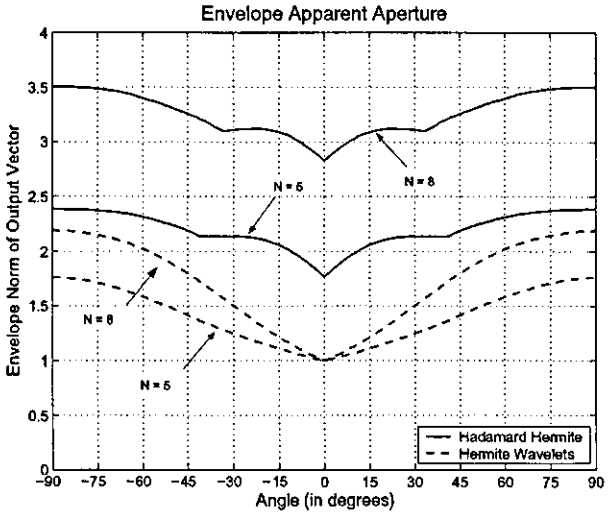

Fig. 2. Apparent array size envelopes with Hermite and Hadamard-Hermite filters (N = 5 or 8, M = 8).

D. The Signal Covariance Matrix

Finally, we turn our attention to the signal covariance matrix $\mathbf{R}$. If s_k are anyhow correlated, $\mathbf{R}_s$ is rank-deficient. This can result, for instance, from dense and unresolvable multipath propagation. In this most general case, estimating the number of sources, their respective DoAs and delays would require maximum likelihood techniques such as [19].

Within the theory of UWB-IR, however, multipath is a rather circumstantial problem, which remains only so long as pulses of short enough duration cannot be produced, given the limitations of existing hardware technology. In fact, the very idea behind the UWB-IR concept is to operate with pulses short enough "that multipath is resolvable down to path differential delays and on the other of a nanosecond or less, *i.e.*, down to path length differentials on the order of a foot or less, [which] significantly reduces fading effects even in indoor environments," - as put by Win and Scholtz in [21]. Recent channel measurements using very short pulses [24] have shown that, indeed, the average number of paths per delay-bin (wavelength) observed in the UWB-IR channel is rather small (approximately 1 path/bin with omnidirectional bi-conic antennas both in and out line-of-sight). Although the number of physical paths contributing to each delay-bin is rather difficult to measure, further evidence supporting this fact is provided in , where it is shown that the fading processes of the strongest delay-bins follow the Log-norm or the Rice distributions.

The rank deficiency of $\mathbf{R}_s$ can, nevertheless, result if each RAKE finger captures the signals of more sources than the number of antenna elements available, *i.e.*, $K > N$.

In addition to the less important case of multi-user scenarios (it is unlikely the the techniques discussed are used in UWB-IR networks), this could accurately describes the scenario faced by channel sounding set-ups in environments with large delay spreads using direct sequence spread (DS) transmission technique, where pulses are transmitted at a very high rate (nearly unitary duty cycle), modulated by long orthogonal digital sequences [25].

In both of the cases depicted above, cumulant-based parameter estimation methods could be employed in UWB-IR array antennas with the construction here proposed [20], which not only can handle a larger number of sources than the number of available antenna elements, but also is less sensitive to correlation amongst different sources. This is currently being investigated by the authors.

Finally, the simpler case when $K < N$ and s_k are fully uncorrelated symbols, though not realistic in narrowband communications, is of practical interest in UWB-IR. This scenario accurately describes outdoor environments, especially in UWB-IR systems where severe restrictions on transmit power effectively limits application to short-range, line-of-sight (LoS) conditions. In this case, $\mathbf{R}_s$ reduces to a diagonal matrix (therefore positive definite and full-rank) with the powers of the k signals along the main diagonal, such that DoA and delay estimation are easily obtained using well-known, and relatively low-complexity algorithms [18].

IV. Examples: Capon Beamformer and MUSIC Algorithms

The objective of this paper is to illustrate *how* the introduction of orthonormal correlation filters enables well-known parameter estimation techniques to be utilized in UWB-IR systems, rather than discuss *which* particular algorithm is best in any scenario. We shall, therefore, limit the examples given in this section to two fairly simple and classical algorithms, namely, the Capon Beamformer and the MUSIC Algorithm [18]. Other algorithms can potentially be employed, as mentioned in section III-D. Let us only add that there are, nevertheless, several techniques which cannot be employed (at least in a straightforward fashion). To cite a few examples, Spatial Smoothing as well as the ESPRIT and the Root-MUSIC algorithms cannot be used, since they depend on structures not preserved in the vectors given by equations (5) or (15).

Hereafter it is assumed that DoAs and delays of the signals collected by a certain RAKE finger are to be estimated within a given space-time window Ω, defined by the limits $\theta_{\min} = 0°$, $\theta_{\max} = 180°$, $\tau_{\min} = -T/2$ and $\tau_{\max} = T/2$.

a) The Capon Beamformer

In the Capon beamformer [18], Ω is scanned using an the following optimum weight vector computed for every point (θ, τ)

$$\chi = \min_{\mathbf{x}} \left(\mathbf{x}^{\mathrm{T}} \cdot \mathbf{R} \cdot \mathbf{x} \right) \text{ subject to } \left| \mathbf{x}^{\mathrm{T}} \cdot \mathbf{a}(\theta, \tau) \right| = 1. \quad (22)$$

Note that the search vector $\mathbf{a}(\theta, \tau)$ has the same form as in equation (5). We only explicitly included the arguments (θ, τ) so as to emphasize the dependence of $\mathbf{a}$ on these variables.

The general solution of equation (22) is given below and depends only on the positive definiteness of $\mathbf{R}$ [18].

$$\chi = \frac{\mathbf{R}^{-1} \cdot \mathbf{a}(\theta, \tau)}{\mathbf{a}(\theta, \tau)^{\mathrm{T}} \mathbf{R}^{-1} \cdot \mathbf{a}(\theta, \tau)} \quad (23)$$

Given that $\mathbf{S}$ has full rank, the positive definiteness of $\mathbf{R}$ depends on the linear independence of the rows of $\mathbf{A}$, which is hard to determine explicitly due to the complexity of the correlation functions $R_{n,m}(\tau)$. However, we note that the K uncorrelated sources cannot be at the same point in Ω and τ_k's are (finger-wise) limited by the RAKE structure. The rows of $\mathbf{A}$ are then non-zero samples of the non-linear independent functions $R_{n,m}(\tau)$ and, therefore, approach random samples of independent processes.

It follows that the rows of $\mathbf{A}$ are linearly independent and equation (23) holds and. The Capon beamformer is therefore straightforwardly applicable, and its spectrum is given by [18]

$$P_{\text{Capon}}(\theta, \tau) = \frac{1}{\mathbf{a}(\theta, \tau)^{\mathrm{T}} \mathbf{R}^{-1} \cdot \mathbf{a}(\theta, \tau)}. \quad (24)$$

b) The MUSIC Algorithm

It is clear from the above that the array covariance matrix of equation (11) satisfies the conditions for using the MUSIC algorithm (in addition to being positive definite, $\mathbf{R}$ is real and symmetric, thus Hermitian). Let us add that the choice for orthonormal correlators at different elements is especially crucial to subspace-based techniques in order to preserve the orthogonality between the noise and the signal subspaces.

The MUSIC algorithm is obtained straightforwardly, by taking the eigen-decomposition of $\mathbf{R}$, extracting the basis of the noise subspace (given by the smallest $N - K$ eigenvectors) and computing its projection onto the signal subspace [18].

Let $\mathbf{v}_n$ denote the n-th eigenvector of $\mathbf{R}$ and, without loss of generality, associate the first largest eigen-vectors $\mathbf{v}_{n=0,\cdots,K-1}$ to the signal subspace. Then, the basis of the noise subspace and the MUSIC spectrum are respectively given by

$$\mathbf{V} = [\mathbf{v}_K \ \mathbf{v}_{K+1} \ \cdots \ \mathbf{v}_{N-1}] \quad (25)$$

$$P_{\text{MUSIC}}(\theta, \tau) = \frac{1}{(\mathbf{a}(\theta, \tau)^{\mathrm{T}} \cdot \mathbf{V}) \cdot (\mathbf{V}^{\mathrm{T}} \cdot \mathbf{a}(\theta, \tau))}. \quad (26)$$

V. Simulation Results

In section a few simulation results obtained with the algorithms described above are given. The simulated scenario had independent sources, A and B, with associated DoA and TDoA given by $(-30°, -0.4)$ and $(15°, 0.3)$, respectively, where DoAs are in degrees and relative delays are in units of the pulse-width. An 8-element ULA of length $\lambda/2$ with the proposed orthonormal Hadamard-Hermite templates constructed with $M = 8$ was used to estimate the location of the sources.

Figures 3 and 4 show top views of the MUSIC and Capon spectra, respectively, obtained with an SNR (at the output of the correlators) of 10 dB. The figures indicate that both methods were capable of yielding correct estimates of the source location. In figure 5, the projections of the Capon and the MUSIC spectra are shown superimposed in the same plot for comparison of their performances. Solid lines are for DoA spectra and dashed lines are for delay spectra, with associated markers given at the bottom and the top of plot, respectively.

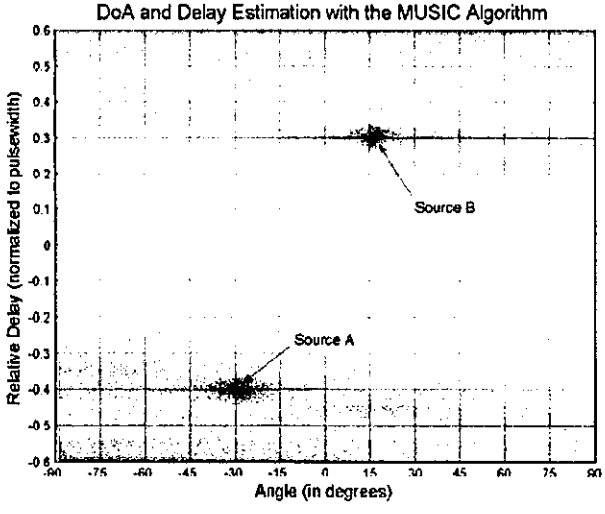

Fig. 3. Top view of 2D MUSIC spectrum with Hadamard-Hermite array.

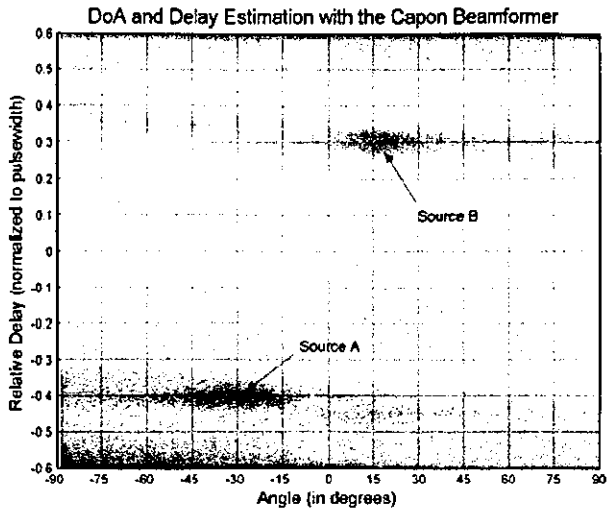

Fig. 4. Top view of 2D Capon spectrum with Hadamard-Hermite array.

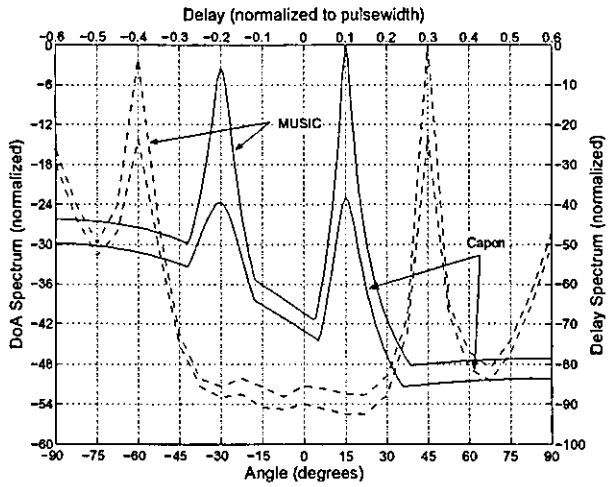

Fig. 5. Superimposed projections of 2D Capon and MUSIC spectra.

The results illustrate that, as expected, the resolution of the MUSIC algorithm is superior to that of the Capon beamformer, suggesting that subspace-based algorithms outperform beamforming-based techniques, as commonly found in narrowband array applications.

VI. Conclusions

We have shown that some well-known narrow-band array antenna techniques for parametric estimation of positioning information can be employed almost straightforwardly to UWB-IR systems if orthonormal correlation filters are used across the array. The technique can potentially be used to build equipment for directive sounding of the UWB-IR channel.

References

[1] M. R. Walton and H. E. Hanrahan, "Hermite wavelets for multicarrier data transmission," in *Proc. IEEE South African Symposium on Communications and Signal Processing*, Jan Smuts Airport, South Africa, Aug.6 1993.

[2] R. J.-M. Cramer, R. A. Scholtz, and M. Z. Win, "On the analysis of UWB communication channels," in *Proc. Military Communications Conference (Milcom'99)*, vol. 2, Atlantic City, NJ, Nov. 1999, pp. 1191–1195.

[3] M. Ghavami, L. B. Michael, and R. Kohno, "A novel uwb pulse shape modulation system," *Kluwer International Journal on Wireless Personal Communications*, vol. 23, no. 1, pp. 105–120, Aug. 2002.

[4] J. A. N. da Silva and M. L. R. de Campos, "Orthogonal pulse shape modulation for impulse radio," in *Proc. IEEE International Telecommunications Symposium (ITS'02)*, Natal, Brazil, Sept. 2002, pp. 916–921.

[5] M. Pinchas and B. Z. Bobrovsky, "Orthogonal laguerre polynomial pulses for ultra-wideband communications," in *Proc. IEEE International Workshop on Ultra-Wideband Systems (IWUWBS'03)*, Oulu, Finland, June 2003.

[6] R. Dilmaghani, M. Ghavami, B. Allen, and H. Aghvami, "Novel uwb pulse shaping using prolate spheroidal wave functions," in *Proc. IEEE* $14^{t}h$ *International Symposium on Personal, Indoor and Mobile Radio Communications (PIMRC'03)*, Beijing, China, Sept.7-10 2003.

[7] J.-B. Martens, "The hermite transform-theory," *IEEE Trans. Acoust., Speech, Signal Processing*, vol. 38, no. 9, pp. 1595–1606, Sept. 1990.

[8] L. R. L. Conte, R. Merletti, and G. V. Sandri, "Hermite expensions of compact support waveforms: Applications to myoelectric signals," *IEEE Trans. Bio-Med. Eng.*, vol. 41, no. 12, pp. 1147–1159, Dec. 1994.

[9] M. R. Mackenzie and A. K. Tieu, "Hermite neural network correlation and application," *IEEE Trans. Signal Processing*, vol. 51, no. 12, pp. 3210–3219, Dec. 2003.

[10] C. J. Mitchell, G. T. F. de Abreu, and R. Kohno, "Combined pulse shape and pulse position modulation for high data rate transmissions in uwb communications," *International Journal of Wireless Information Network - Special Issue on UWB*, vol. 11, Apr. 2004.

[11] M. Hämäläinen, R. Tesi, V. Hovinen, N. Laine, and J. linatti, "Ultra wideband system performance studies in awgn channel with intentional interference," in *Proc. IEEE International Workshop on Ultra-Wideband Systems (IWUWBS'03)*, Oulu, Finland, June 2003.

[12] G. T. F. de Abreu, C. J. Mitchell, and R. Kohno, "On the design of orthogonal pulse-shape modulation for uwb systems using hermite pulses," *Journal of Communications and Networks - Special Issue on Ultra-Wideband Communications*, vol. 5, no. 4, pp. 328–343, Dec. 2003.

[13] ——, "Jitter-robust orthogonal hermite pulses for ultra wideband impulse radio communications," *EURASIP Journal on Applied Signal Processing*, 2004, to appear - 4th quarter.

[14] G. T. F. de Abreu, "Closed-form correlation functions of generalized hermite wavelets," *IEEE Trans. Signal Processing*, 2004, submitted.

[15] R. A. Scholtz and M. Z. Win, "Impulse radio," in *Wireless Communications: TDMA versus CDMA*, S. G. Glisic and P. A. Leppanen, Eds. Kluwer Academic Publishers, 1997, ch. 7, pp. 245–267.

[16] A. Armogida, B. Allen, M. Ghavami, M. Porretta, G. Manara, and H. Aghvami, "Path loss modelling in short-range uwb transmissions," in *Proc. IEEE International Workshop on Ultra-Wideband Systems (IWUWBS'03)*, Oulu, Finland, June 2003.

[17] A. D. Poularikas, *The Transforms and Applications Handbook, Second Edition*, 2nd ed. CRC Press, Feb.23 2000.

[18] S. U. Pillai and C. S. Burrus, *Array Signal Processing*. New York, NY: Springer Verlag, May 1989.

[19] C. M. Tan, M. A. Beach, and A. R. Nix, "Enhanced-sage algorithm for use in distributed-source environments," *IEEE Signal Processing Lett.*, vol. 39, pp. 697 – 698, Apr. 2003.

[20] Z. Shan, F. Ji, and G. Wei, "Extending music-like algorithm for doa estimation with more sources than sensors," in *Proc. IEEE International Conference on Neural Networks & Signal Processing*, vol. 2, Nanjing, China, Dec.14-17 2003, pp. 1281 – 1284.

[21] M. Z. Win and R. A. Scholtz, "Ultra-wide bandwidth time-hopping spread-spectrum impulse radio for wireless multiple-access communications," *IEEE Trans. Commun.*, vol. 48, no. 4, pp. 679–691, Apr. 2000.

[22] J. G. Proakis, *Digital Communications, Fourth Edition*. New York, NY: Mc-Graw-Hill, 2000.

[23] K. Arasu and J. Seberry, "On circulant weighing matrices," *Australasian Journal of Combinatorics*, pp. 21–37, 1998. [Online]. Available: citeseer.ist.psu.edu/arasu98circulant.html

[24] D. R. McKinstry and R. M. Buehrer, "Uwb small scale channel modeling and system performance," in *Proc. IEEE 58st Vehicular Technology Conference (VTC'03 Fall)*, vol. 1, Orlando, FL, U.S.A., Oct.6-9 2003, pp. 6–10.

[25] Q. Li and L. A. Rusch, "Multiuser detection for ds-cdma uwb in the home environment," *IEEE J. Select. Areas Commun.*, vol. 20, pp. 1701 – 1711, Dec. 2002.

International Symposium on Information Theory and its Applications, ISITA2004
Parma, Italy, October 10–13, 2004

Maximum Likelihood Estimation of Trellis Encoder and Modulator Transition Utilizing HMM for Adaptive Channel Coding and Modulation Technique

Kentaro IKEMOTO† and Ryuji KOHNO†

† Graduate School of Engineering,
Yokohama National University, Yokohama, 240-8501 Japan.
E-mail: ikemoto@kohnolab.dnj.ynu.ac.jp and kohno@ynu.ac.jp

Abstract

In order to achieve adaptive channel coding and adaptive modulation, the main causes of degradation to system performance are the decoder selection error and modulation estimation error. The utilization of supplementary information, in an estimation system utilizing channel estimation results, blind modulation estimation, and blind encoder estimation using several decoders information and encoder transitions have been considered to overcome these two problems. There are many issues in these methods, however, such as the channel estimation difference between transmitter and receiver, computational complexity and the assumption of perfect CSI. Our proposal, on the other hand, decreases decoder and modulation selection error using a Hidden-Markov Model (HMM). In order to estimate the switching patterns of the encoder and modulator, our proposed system selects the maximum likelihood encoder and modulation transition patterns using both encoder and modulation transition probability based on the HMM obtained by CSI and also Encoder and Modulation Selection Error probabilities. Therefore, the decoder and demodulation results can be achieved efficiently without any restraint on the pattern of switching encoder and modulation.

1. Introduction

Recently, there has been a growing amount of research into mobile communications, especially adaptive algorithms that can achieve optimal system constructions considering time and/or geographic environmental problems as well as an adaptive algorithm that adjusts the constructions in order to satisfy users needs. One of the research topics, which has attracted much attention, is adaptive channel coding and the adaptive modulation scheme [1]. The aim of this research is to alter encoders or modulators in order to achieve the desired performance.

On the other hand, to change the encoders and modulators, it is necessary to design a pattern for transmitter and receiver. Therefore, along with the problem that poor decoding performance occurs due to error in selection of decoders and demodulators, the sequence synchronization problem that occurs due to the utilization of several decoders with different coding rates or different modulation orders is also a crucial problem.

In order to solve these problems, there are two main methods [2–6]. One is to add supplemental information at the transmitter to indicate which encoder and modulation scheme are being used, the other is to estimate which encoder and modulation scheme are used at the receiver using the decoder and demodulator results. In the first case, in order to prevent error in the supplementary information, error correction codes with high quality are needed. However, longer redundancy causes lower transmission rates, and this rate becomes even lower when the encoder and modulator are changed frequently. Additionally, one can consider using pilot symbols to choose encoder and modulator, however, this method requires perfect channel estimation, or a not appropriate decoder and demodulator can be selected. On the other hand, in the latter case, the minimum distance between encoders determines encoder estimation accuracy. Just as with the minimum distance between codewords, the longer the distance, the better the performance. Due to the limited choices of encoder, it is hard to change the estimation accuracy adaptively. Moreover, modulation estimation accuracy depends on the distance between any two of the constellation points.

Moreover, the encoding method considering a finite state machine utilizing the fading channel model has also been studied [7]. However, this method cannot accommodate all the channel models. In order to solve this problem, we focus on HMM. Fading channel-modeling schemes using HMM have been widely studied recently, and we propose a scheme using this kind of channel modeling to encode and modulate. Our pro-

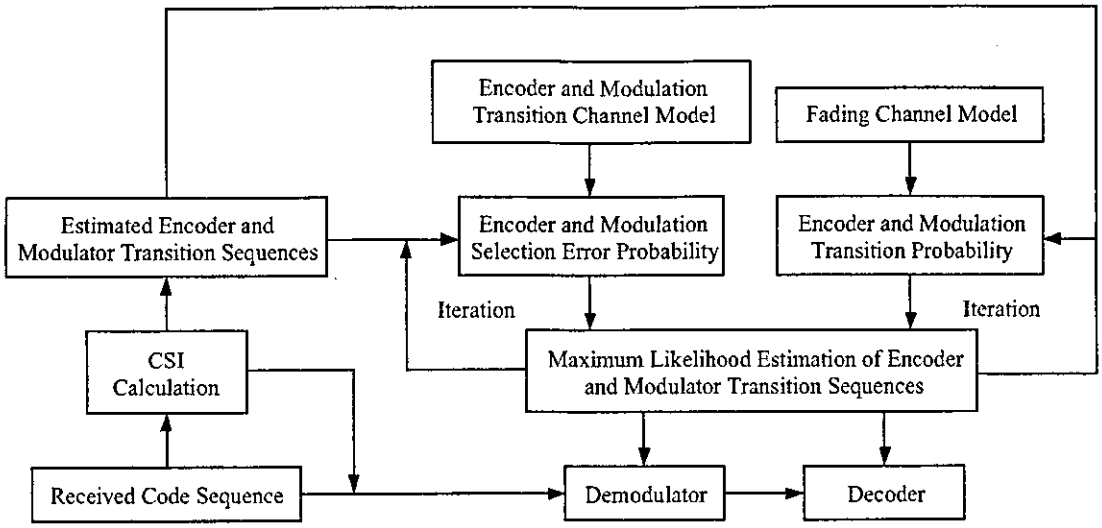

Figure 1: System Model

posals performance deteriorates when the channel estimations at transmitter and receiver are different, or if the estimation of encoder and modulator at the receiver is invalid. Consequently, we additionally add an algorithm to our proposal to reduce decoder and modulator selection errors using the HMM.

In more detail, our proposed system selects the maximum likelihood encoder and modulation transition by using both encoder and modulation transition probabilities based on the HMM obtained using CSI and Encoder and Modulation Selection Error probabilities. We use Expectation-Maximization (EM) algorithm [8] as a maximum likelihood algorithm, and this proposal can be realistically achieved with computational complexity relying only on the number of trellis states, which is different from the conventional system. Comparing to a conventional finite state machine scheme whose transition pattern and encoder or modulator switching pattern have a one to one correspondence, the proposed HMM scheme whose transition pattern is probabilistically determined is more efficient in a fading channel. Therefore, the decoder and demodulation results can be achieved efficiently without any restraint on the pattern of encoder and modulation switching.

This paper is organized as follows. In section 2., considering our proposed adaptive coding and modulation scheme under HMM, we show the encoder and modulator switching estimation schemes with maximum likelihood in more detail. In section 3., the performance of the proposed system using computer simulations is shown. Finally, we conclude this paper in section 4..

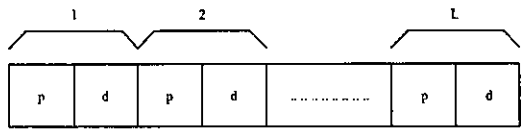

Figure 2: Frame Structure of received data for fading channel

2. Adaptive coding and modulation scheme using HMM

2.1. System Model

The transmit sequence is shown in Fig.2. We assume a TDD system with L frames, and each frame consists of d transmit bits plus p pilot symbols for channel estimation. According to the channel estimation result, appropriate encoder and modulator are selected for the information sequence. Notice that the channel model is HMM. Fig.1 shows the proposed system block diagram. Fig.3 shows the flowchart of our proposed system.

In Fig.3, after estimating the channel with the p received pilot symbols in Step 1, the result is used to estimate the encoder and modulator as well as the received sequence compensation. With the selected encoder and modulator in Step 2, the encoder and modulator switching pattern is constructed to obtain a switching

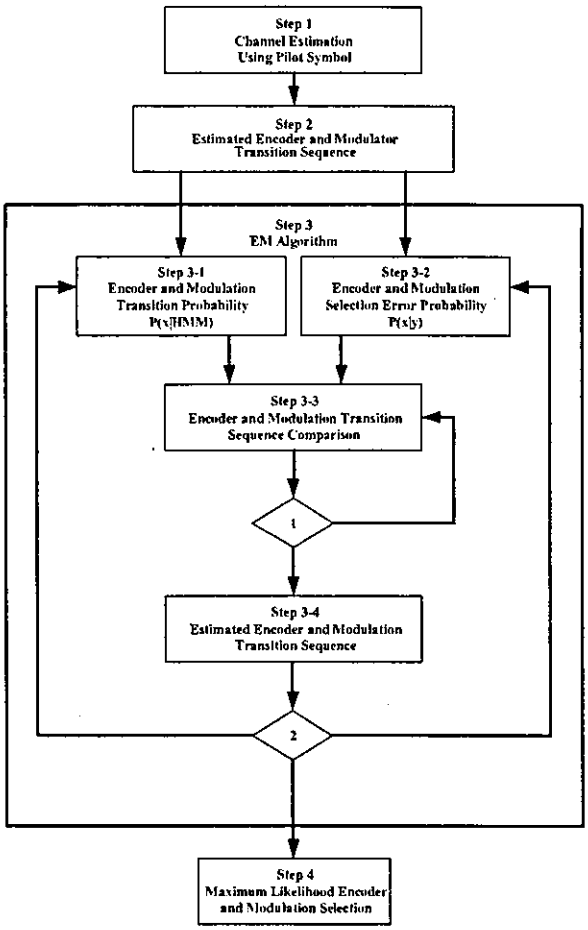

Figure 3: Flowchart of our proposed system

pattern probability using the BCJR algorithm in Step 3-1. Additionally, the probability of decoder and demodulator selection errors is extracted using CSI and selected encoder and modulator in Step 3-2. With these two probabilities, iterative maximum likelihood estimation is implemented to find a more appropriate encoder and modulator switching pattern in Step 3-3 and 3-4.

2.2. Definition of maximum likelihood estimation of encoder and modulator switching patterns

This section describes how to define the maximum likelihood encoder and modulation selection, Step 4. When HMM is used as a probabilistic model for encoder and modulator switching pattern, this model has the possibility to derive the conditional probability $P(\hat{x}|HMM)$ (Step 3-1) using the BCJR algorithm, where $\hat{x} = (x_1, x_2, \cdots, x_t, \cdots, x_{N_t})$ represents the switching pattern sequence. Defining $P(\hat{x}|\hat{y})$ (Step 3-2) as the conditional probability that the estimated switching pattern $\hat{y}$ at receiver provides a value close to $\hat{x}$, $P(\hat{x}|\hat{y})$ can be derived from CSI or decoder and demodulator selective errors based on the selected encoder and modulator. Moreover, to find the optimum sequence $\hat{x}$ from both of these probabilities leads to a maximum likelihood estimation of the encoder and modulator switching pattern.

2.3. Extraction of the probability of encoder and modulator switching pattern

The conditional probability $P(\hat{x}|HMM)$ of encoder and modulator switching pattern sequence $\hat{x}$ when it is HMM can be easily derived by BCJR algorithm due to the utilization of HMM model. Notice that we use normalized BCJR algorithm that considers underflow problem. Let us define the forward metric as $\alpha_t(s)$, and the backward metric as $\beta_t(s)$. Assume the channel condition is the same as HMM, the transition probability from state s to state $\acute{s}$ is $p_{s\acute{s}}$, and according to this transition, $p_{s\acute{s}}(\hat{x}_t)$ represents the probability when selected encoder and modulator pattern is transformed to be a code x_t. Note that there are N states, where N=1, $\cdots$, N_s. $\alpha_t(s)$ and $\beta_t(s)$ are given by (1) and (2), and calculated recursively.

$$\alpha_t(\acute{s}) = \sum_{s=1}^{N_s} \alpha_{t-1}(s) p_{s\acute{s}} p_{s\acute{s}}(\hat{x}_t) \tag{1}$$

$$\beta_t(\acute{s}) = \sum_{s=1}^{N_s} \beta_{t+1}(s) p_{s\acute{s}} p_{s\acute{s}}(\hat{x}_{t+1}) \tag{2}$$

The initial values are $\alpha_1(s) = (\pi_1, \pi_2, \cdots, \pi_N)$, where $\sum_{s=1}^{N} \pi_s = 1$ and $\beta_N(s) = 1$, respectively, and due to the necessity of normalization, (3) and (4) are used.

$$\bar{\alpha}_t(\acute{s}) = \frac{1}{\sum_{\acute{s}=1}^{N_s} \alpha_t(\acute{s})} \alpha_t(\acute{s}) \tag{3}$$

$$\bar{\beta}_t(\acute{s}) = \frac{1}{\sum_{\acute{s}=1}^{N_s} \beta_t(\acute{s})} \beta_t(\acute{s}) \tag{4}$$

Then $P(\hat{x}|HMM)$ is given by (5).

$$P(\hat{x}|HMM) = \sum_{s=1}^{N_s} \alpha_{t-1}(s) \cdot \sum_{\acute{s}=1}^{N_s} \beta_t(s) \cdot \sum_{s=1}^{N_s} \sum_{\acute{s}=1}^{N_s} \bar{\alpha}_{t-1}(s) p_{s\acute{s}} p_{s\acute{s}}(\hat{x}_t) \bar{\beta}_t(\acute{s}) \tag{5}$$

2.4. Extraction of decoder and demodulator selective error probability

Define $P(\hat{x}|\hat{y})$ as the probability of sequence $\hat{x}$ when the received encoder and modulator switching pattern sequence is $\hat{y}$. $P(\hat{x}|\hat{y})$ belongs to binary symmetric channel, and given by,

$$P(\hat{x}|\hat{y}) = p^d(1-p)^{n-d} \tag{6}$$

where p represents the decoder or demodulator selective error, d is the number of these errors and also can be described as the hamming distance between $\hat{x}$ and $\hat{y}$ and n is the length of encoder and modulator switching pattern sequence.

2.5. Maximum likelihood estimation scheme for encoder and modulator selection

We focus our attention on seeking a sequence $\hat{x}$ that maximizes both $P(\hat{x}|HMM)$ and $P(\hat{x}|\hat{y})$. We adopt EM algorithm for our proposal. Step 3 in Fig.3 indicates this algorithm. EM algorithm is a broadly applicable approach to the iterative computation of maximum likelihood estimates, useful in a variety of incomplete-data problem. On each iteration of the EM algorithm, there are two steps called the expectation step or the E-step and the maximization step or the M-step. Define $\hat{x}_t^i$ as the sequence of estimated encoder or modulator switching pattern in i-th iteration and t-th time slot. In E-step, $P(\bar{x}_{inv}^i)$ is derived by multiplying $P(\bar{x}|HMM)$ by $P(\bar{x}|\hat{y})$. Let $\bar{x}_{inv}^i$ (inv=1, $\cdots$, N_t) be the code sequence whose code sign at inv-th time slot is inverted from original code sequence constructed from encoder and modulator, and substitute to (7) to obtain N_t sequences, thus N_t probabilities of $P(\bar{x}_{inv}^i)$. In M-step, each of N_t probabilities, $P(\bar{x}_{inv}^i)$, is compared to the original sequence $P(\hat{x}^i)$, and we invert the code sign at all the time slots whose probability $P(\bar{x}_{inv}^i)$ is larger than the original sequence probability $P(\hat{x}^i)$, thus obtain one sequence $P(\hat{x}^{i+1})$. (8) indicates the M-step algorithm, where T represents the transpose. In next iteration, $P(\bar{x}_{inv}^{i+1}|HMM)$ and $P(\bar{x}_{inv}^{i+1}|\hat{y})$ are extracted again using (5) and (6), and then substituted to (7) and (8). After several iterations until the convergence of $P(\hat{x}^{i+1})$, $\hat{x}^{i+1}$ is considered to be the maximum likelihood encoder and modulator selections.

$$P(\bar{x}_{inv}^i) = P(\bar{x}_{inv}^i|HMM) \cdot P(\bar{x}_{inv}^i|\hat{y}) \tag{7}$$

$$\begin{aligned} P(\hat{x}^{i+1}) &= (P(\hat{x}_1^{i+1}), P(\hat{x}_2^{i+1}), \cdots, P(\hat{x}_t^{i+1}), \\ &\quad \cdots, P(\hat{x}_{N_t}^{i+1})) \\ &= \begin{pmatrix} \arg\max(P(\bar{x}_1^i), P(\hat{x}^i)), \\ \arg\max(P(\bar{x}_2^i), P(\hat{x}^i)), \\ \vdots \\ \arg\max(P(\bar{x}_{inv}^i), P(\hat{x}^i)), \\ \vdots \\ \arg\max(P(\bar{x}_{N_t}^i), P(\hat{x}^i)) \end{pmatrix}^T \end{aligned} \tag{8}$$

3. Computer Evaluation

We show the reduction of decoder and demodulator selective errors in order to clarify the effectiveness of our proposal.

3.1. Prerequisite

Assuming that the fading channels are defined by HMM, and AWGN channels. The transition probability $p_{s\acute{s}}$ from state s to $\acute{s}$, and the probability $p_{s\acute{s}}(x_t)$ that $p_{s\acute{s}}$ transforms the encoder and modulator selected based on this probability to x_t, are considered to be given. Moreover, the synchronization at the receiver is considered to be perfect. The information data is encoded by the encoder selected based on CSI information, and the encoded data $a_i (i = 1, 2, \cdots, n)$ is obtained. Notice that the code lengths are the same even if the code rates or the error correction probabilities are different. The same number of symbols is transmitted for any modulation scheme in each packet. The timing for switching the modulation scheme is determined by synchronizing the packet length of BPSK. Therefore, the modulation scheme is switched by the length of packet which is one frame with BPSK, two frames with QPSK, three frames with 8PSK, and four frames with 16QAM.

3.2. Evaluation of reduction of selective errors

Table 1 shows the simulation parameters. The fading channels rely on HMM, and the state of HMM is 2. Fig.4 shows the trellis diagram and state transition of HMM. The probability $p_{s\acute{s}}$ and $p_{s\acute{s}}(x_t)$, and the code sequence x_t are described in previous subsection and are defined as $p_{00} = 1 - p_{10}$, $p_{01} = 0.06$, $p_{10} = 0.017$, $p_{11} = 1 - p_{01}$, $p_{00}(0) = 0.01$, $p_{01}(0) = 0.5$, $p_{10}(0) = 0.01$, $p_{11}(0) = 0.5$, respectively. Note that 0 represents BPSK modulation scheme, 01 indicates that the modulation scheme is changed from BPSK to QPKS. Considering the combination of encoder and modulator according to HMM states, for simplicity, BPSK and QPSK are used here, and the modulation scheme is changed relying on CNR estimated by CSI. The threshold of switching modulation scheme pattern

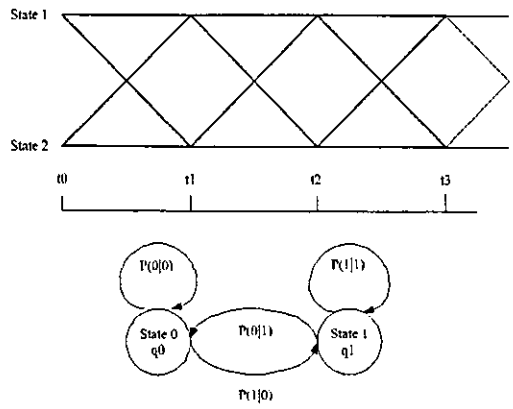

Figure 4: Trellis Diagram and State Transition of HMM

Table 1: Simulation Parameters

Information Length	50
Codeword Length	100
Coding Rate	0.5
Pilot Symbol	10
Modulation	BPSK QPSK
Frame Length	110 (BPSK) 55 (QPSK)
Packet Length	110 Symbols
Encoder and Modulator Switching Sequence Length	25 49, 100
Iteration of EM	1-6

is shown in Table 2. In this case, we desire a BER less than 10^{-4}. Let the information data length be 50 bits, the code rate be $R = 0.5$. Therefore, using convolutional (7, 5) code, the number of encoded bits is 100. The uncoded pilot symbols with bit length 10 are added to each packet, and transmitted with BPSK. The encoder and modulator switching sequence $x_t(x_1, x_2, \cdots, x_{N_t})$ length are considered to be 25, 49, and 100. The number of iteration of EM algorithm is from 1 to 6.

Fig.5-8 show computational evaluation for modulation scheme estimation error. In Fig.5-7, it is seen that the system converges at less than 6-th iteration with EM algorithm. The complexity of proposed system considers $6n$ sequences, while the conventional system selecting all the combinations of any sequence considers 2^n sequences to estimate the most probable sequence. Therefore, the proposed system is effective when $n \geq 5$. Additionally, as far as time permits, the longer the sequence length is, the lower the encoder and modulator selection errors are.

Table 2: Threshold for Adaptive Modulation Scheme

BPSK - QPSK
Es/No=7 (dB)

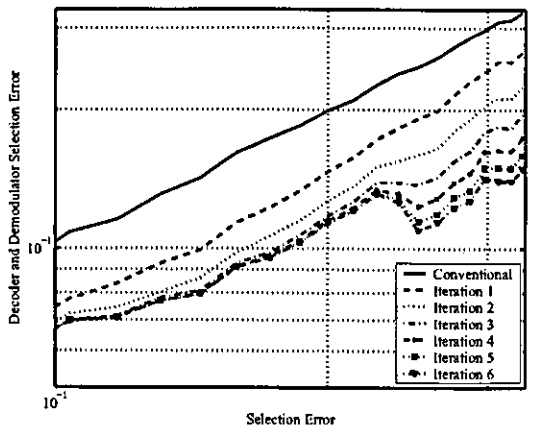

Figure 5: Modulation Selection Error in case switching sequence length is 25

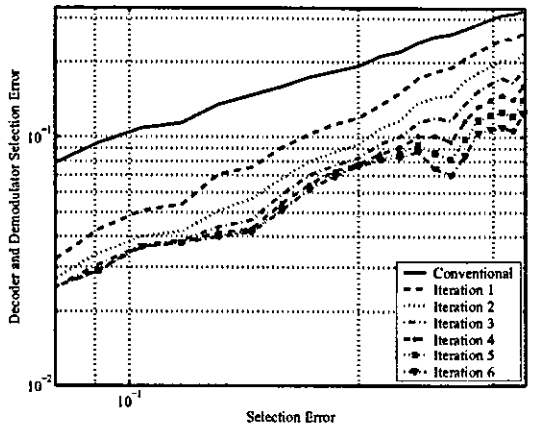

Figure 6: Modulation Selection Error in case switching sequence length is 49

4. Conclusion

In this paper, a reduction of decoder and demodulator selection errors scheme is proposed using HMM

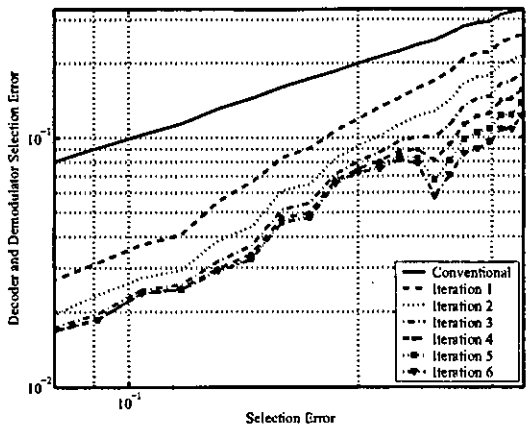

Figure 7: Modulation Selection Error in case switching sequence length is 100

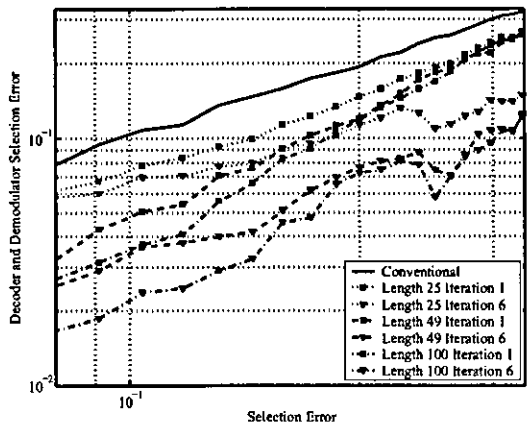

Figure 8: Modulation Selection Error compared with switching sequence length

as an elemental technology to achieve adaptive channel coding and modulation schemes. Based on channel estimation results, the proposal estimates the sequences such as encoder or decoder switching pattern at transmit side using the probabilities of decoder and demodulator selective errors that are obtained by the switching pattern and channel information. Especially, we proposed a maximum likelihood estimation scheme in order to estimate the most likely switching patterns by EM algorithm, and then evaluated the performances by computer simulations. Comparing to the scheme only considering channel estimation results, the proposed scheme achieves better performance, and the computational complexity to search the encoder and modulator switching pattern sequence is lowered from 2^n to $6n$, which is effective when $n \geq 5$. In the future, we will investigate the balance of pilot symbols and information bits, and also the number of encoder or modulator switching pattern sequences that are needed to estimate HMM at the receiver.

References

[1] Hidehiro Matsuoka, Seiichi Sampei and Norihiko Morinaga, "Adaptive Modulation System with Punctured Convolutional Code for High Quality Personal Communication Systems," *IEICE Transactions on Communications*, Vol.E79-B, No.3, pp.328-334, 1996-03

[2] T. Ue, S. Sampei, N. Morinaga and K. Hamaguchi, "Symbol rate and modulation level-controlled adaptive modulation/TDMA/TDD system for high-bit-rate wireless data transmission," *IEEE Trans. Veh. Technol.*, vol.47, no.4, pp.1134-1147, Nov. 1998.

[3] A. Swami and B.M Sadleer, "Hierarchial digital modulation classification using cumulants," *IEEE Trans. Commun.*, vol.48, no.3, pp.416-429, 2000-03

[4] H. Yoshioka, Y. Shirato, M. Nakasugawa and S. Kubota, "Automatic modulation recognition techniques employing the nearest neighbor rule," *IEICE Trans. Commun.* (Japanese Edition), vol.J84-B, no.7, pp.1176-1162, 2001-07.

[5] Kenta Umebayashi, Ryuji Kohno, "Blind Estimation of Modulation Schemes According to Noise Powers in the Presence of Carrier Frequency Offset," *IEICE Transactions on Communications*, vol.J84-B, No.7, pp.1151-1161, 2001-07 (in Japanese)

[6] Kenta Umebayashi, Robert H. Morelos-Zaragoza, Ryuji KOHNO, "Method of Non-Data-Aided Carrier Recovery with Modulation Identification," *IEICE Transactions on Fundamentals of Electronics, Communications and Computer Sciences* Vol.E87-A No.3 pp.656-665, 2004-03

[7] Kentaro Ikemoto, Ryuji Kohno, "Adaptive Channel Coding Scheme Using Finite State Machine For Software Defined Radio," *IEICE Transactions on Communications*, Vol.E85-B, No.12, pp.2663-2671, 2002-12

[8] Geofferey J. McLachlan and Thriyambakam Krishnan, "The EM Algorithm and Extensions," A Wiley-Interscience Publication, JOHN WILEY & SONS, INC., 1996.

International Symposium on Information Theory and its Applications, ISITA2004
Parma, Italy, October 10–13, 2004

Serial Concatenated Coding Schemes over the Space-Time-Frequency Domain for OFDM transmission

Kouji ISHII and Ryuji KOHNO

Div. of Comp. and Elec. and Eng. Faculty of Eng., Yokohama National University,
79-5 Tokiwadai, Hodogaya, Yokohama, Kanagawa, 240-8501, Japan
E-mail: kouji@kohnolab.dnj.ynu.ac.jp,kohno@ynu.ac.jp

Abstract

In this paper, we combine time-frequency error correcting code with space-frequency diversity scheme for wireless OFDM transmissions through time-varying and frequency-selective fading channels. The purpose of concatenation between space-frequency and time-frequency domain codes is to obtain both diversity and coding gains over space-time-frequency domain. We propose the serial concatenated encoding and decoding. Simulations demonstrate that the proposed system leads to significantly enhanced performance. We investigate the optimum structure of inner and outer codes. Moreover, we analyze the computational complexity.

1. INTRODUCTION

In order to realize high-speed wireless communication, it is very important to improve frequency efficiency. One of the techniques which can improve bandwidth efficiency is a space-time coding (STC) [4]-[7]. STC appropriately maps input symbol streams across space and time in order to obtain transmit diversity and coding gain at the transmitter. On the other hand, as a high-speed data transmission technique and a countermeasure technique against inter-symbol interference (ISI), orthogonal frequency division multiplexing (OFDM) has received a lot of attentions. Due to cyclic prefix (CP) insertion, the channel of OFDM transmission can be considered as ISI-free. While, a STC technique is weak against ISI, there is a lot of attention to a combination between STC techniques and OFDM transmission. For high-speed wireless data transmission, space-time coded OFDM transmission is one of the most important techniques.

In this paper, we pay attention to space-time-frequency (STF) coded OFDM transmissions over frequency selective Rayleigh fading channels. There has been a lot of investigation into the design criteria of space-time (ST), space-frequency (SF) and STF codes [4]-[7]. These investigations, however, do not take channel coding into account. In order to realize high-reliability communications, it is necessary to optimize the system considering both an error correcting and a STF (ST, SF) coding technique. In this paper, we propose and investigate a structure of concatenation between SF and time-frequency (TF) domain channel codes. Due to concatenate another domain code, we aim to obtain another domain of both diversity and coding gains. The proposed encoder structure consists of a channel encoder in TF domain and a SF code with an interleaver between each encoder. We consider the channel encoder as the outer encoder and the SF encoder as the inner encoder. Therefore, the proposed encoder structure can be considered as a serial concatenation code between TF and SF encoders. While, the decoder can operate iteratively in time, frequency and space domains. The major contributions of the proposed system are the following.

- For multiantenna OFDM systems through time-varying and frequency-selective Rayleigh fading channels, we can achieve high coding and diversity gain over space, time and frequency.
- We investigate the optimum structure of each element encoder for the proposed coding structure by computer simulations.
- We analyze the computational complexity of the proposed system.

2. STF Coded OFDM Transmission Through Time-Varying and Frequency-Selective Fading Channels

In this section, we describe the system model. Fig. 1 depicts a multi-antenna OFDM transmission model with N_t transmit antennas and N_r receive antennas. One OFDM frame consists of N_c subcarriers and N_s symbols. We define the channel response

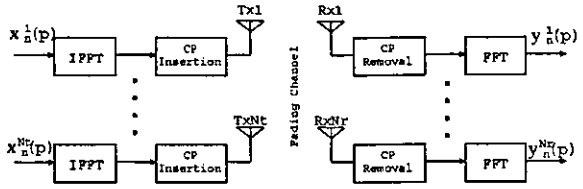

Figure 1: System model of multi-antenna OFDM transmission between the transmit symbols x and the receive symbols y.

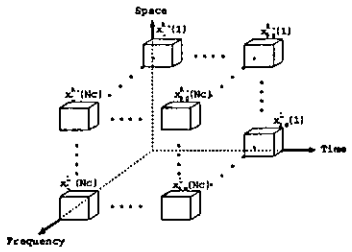

Figure 2: Structure of transmit signal over the space-time-frequency domain.

between the μth transmit antenna and the νth receive antenna at time n as $\mathbf{h}^n_{\mu\nu}$. $\mathbf{h}^n_{\mu\nu}$ is a frequency-selective and time varying channel response described by the discrete-time baseband equivalent impulse response vector $[h^n_{\mu\nu}(0), \cdots, h^n_{\mu\nu}(L)]^T \in \mathbf{C}^{(L+1)\times 1}$, where L stands for the channel order. $x^\mu_n(p)$ shows the data symbol transmitted on the pth ($p \in [1, \cdots, N_c]$) subcarrier from the μth ($\mu \in [1, \cdots, N_t]$) transmit antenna during the nth ($n \in [1, \cdots, N_s]$) OFDM symbol interval. Fig. 2 shows the structure of the transmit symbols over space, time and frequency domains. The transmit symbols are inverse-fast-Fourier-transformed (IFFT), CP inserted and transmitted with each transmit antenna. The length of CP is defined as L. While, at the receiver side, each antenna receives faded signals which are transmitted from multi-antenna. We assume that carrier synchronization and channel estimation are ideal. The receiver removes CP from the received signals and does a fast-Fourier-transform (FFT). As the results of those processes, we get $y^\nu_n(p)$ representing the signal of the νth receive antenna, nth symbol and pth subcarrier. $y^\nu_n(p)$ can be expressed as

$$\begin{aligned} y^\nu_n(p) &= \sum_{\mu=1}^{N_t} H^n_{\mu\nu}(p) x^\mu_n(p) + \omega^\nu_n \qquad (1) \\ \nu &= 1, \cdots N_r \\ n &= 1, \cdots N_s \\ p &= 1, \cdots N_c \end{aligned}$$

where $H^n_{\mu\nu}(p)$ is the channel gain of pth subcarrier nth symbol from the μth transmit antenna to the νth receive antenna, and ω^ν_n is the complex additive white Gaussian noise (AWGN) of νth receive antenna, nth symbol and pth subcarrier with zero mean and variance N_0. $H^n_{\mu\nu}(p)$ is defined as

$$H^n_{\mu\nu} = \sum_{l=0}^{L} h^n_{\mu\nu}(l) e^{-j(2\pi/N_c)lp}. \qquad (2)$$

Equation (1) can be rewritten in a 3-D matrix as follows;

$$\mathbf{Y}(p) = \mathbf{H}(p)\mathbf{X}(p) + \mathbf{W}(p). \qquad (3)$$

Equation (3) shows the MIMO OFDM transmission system with N_t transmit antenna, N_r receive antenna, N_c subcarriers and N_s symbols. The received signal matrix $\mathbf{Y}$ over STF domains is given by

$$\mathbf{Y} = [\mathbf{Y}(1), \cdots, \mathbf{Y}(N_c)] \in \mathbf{C}^{N_r \times N_s \times N_c} \qquad (4)$$

where

$$\mathbf{Y}(p) = \begin{bmatrix} y^1_1(p) & \cdots & y^1_{N_s}(p) \\ \vdots & \ddots & \vdots \\ y^{N_r}_1(p) & \cdots & y^{N_r}_{N_s}(p) \end{bmatrix} \in \mathbf{C}^{N_r \times N_s}. \qquad (5)$$

The transmit symbol matrix $\mathbf{X}$, which is encoded over STF domains is given by

$$\mathbf{X} = [\mathbf{X}(1), \cdots, \mathbf{X}(N_c)]^T \in \mathbf{C}^{N_t \times N_s \times N_c} \qquad (6)$$

where

$$\mathbf{X}(p) = \begin{bmatrix} x^1_1(p) & \cdots & x^1_{N_s}(p) \\ \vdots & \ddots & \vdots \\ x^{N_t}_1(p) & \cdots & x^{N_t}_{N_s}(p) \end{bmatrix} \in \mathbf{C}^{N_t \times N_s}. \qquad (7)$$

$\mathbf{H}(p)$ shows the frequency-selective and time variant multi-carrier MIMO channel matrix ($\mathbf{H}(p) \in \mathbf{C}^{Nr \times N_t \times N_s}$) with (ν, μ, n)th entry $[\mathbf{H}(p)]_{\nu\mu n} = H^n_{\nu\mu}(p)$. In this paper, we propose and investigate the way to obtain the encoded signal $\mathbf{X}$ and decode the receive signal $\mathbf{Y}$.

3. Concatenated scheme with time-frequency and space-frequency domain codes

3.1. Concatenated encoding scheme over STF domains

In this subsection, we describe the structure of the proposed concatenated code consisting of a TF domain error correcting code and a SF code. We recall that the channel is a time-varying and frequency-selective Rayleigh fading channel with channel order of length L. We consider the channel as an ISI-free channel, because the length of CP is L. Therefore in this paper

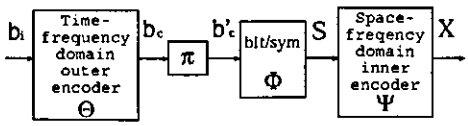

Figure 3: Block diagram of proposed concatenated encoder between a time-frequency and a space-frequency domain codes.

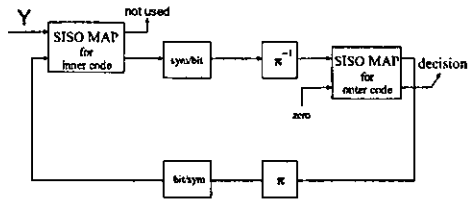

Figure 4: Iterative decoder structure for space-time-frequency domain serial concatenated coded OFDM.

we do not take multipath diversity techniques [6] into account.

Fig. 3 shows the block diagram of the proposed serial concatenated encoder. First, the binary information data $\mathbf{b}_i$ are encoded to the binary data $\mathbf{b}_c$ by a channel (outer) encoder Θ over the TF domain, as follows:

$$\Theta : \mathbf{b}_i \rightarrow \mathbf{b}_c \tag{8}$$

where $\mathbf{b}_i \in \mathbf{C}^k, \mathbf{b}_c \in \mathbf{C}^n$. Therefore, the rate r_c of the outer code in TF domains is $R_{ch} = \frac{k}{n}$. Second, the coded data is interleaved as follows:

$$\pi : \mathbf{b}_c \rightarrow \mathbf{b}'_c \tag{9}$$

where π is defined as the interleaver function and $\mathbf{b}'_c \in \mathbf{C}^n$. Third, the interleaved data $\mathbf{b}'_c$ is mapped to constellation point $\mathbf{S}$, and SF coded as follows:

$$\Phi \ : \ \mathbf{b}'_c \rightarrow \mathbf{S} \tag{10}$$

$$\Psi \ : \ S \rightarrow \mathbf{X} \tag{11}$$

where $\mathbf{S}$ is the modulated symbol, $\mathbf{X}$ is the transmit symbol set, Φ is the mapping function from binary to symbol and Ψ is SF mapping function. $\mathbf{S}$ is chosen from $\mathcal{A}_X$ (in the case of QPSK transmissions, $\mathcal{A}_X$ belongs to [0,1,2,3]). The μth transmit antenna nth symbol interval pth subcarrier transmit signal $[\mathbf{X}]_{\mu np}$ is also chosen from $\mathcal{A}_X$. $|\mathcal{A}_X|$ is the cardinality of $\mathcal{A}_X$. The transmit rate is therefore $R_T = R_{ch} \log_2 |\mathcal{A}_X|$ bit/sec/Hz in the case that we ignore the decrease in the transmission rate due to inserting the pilot signal and CP. Finally, the encoded signals $\mathbf{X}$ are OFDM-modulated (derived by IFFT), CP inserted and transmitted using multiple transmit antennas.

3.2. Iterative decoding scheme

In this subsection, we describe the iterative decoding scheme which can obtain maximum coding and diversity gains over the STF domains. Fig. 4 shows the proposed iterative decoder structure. For the sake of simplicity, we omit the FFT branch and the cyclic prefix remover in fig. 4. Fig. 4 shows the latter part of fig. 1. Recall that the input of the iterative decoder is $\mathbf{Y}$. Therefore, the iterative decoder estimates the information data from the received signal matrix $\mathbf{Y}$.

We give an overview of the decoding process as follows. First, the symbol-symbol MAP decoder for the inner code computes the *extrinsic information* using the LLRs and the *a priori probability*. In the case of the first iteration, the *a priori probability* is $\frac{1}{|\mathcal{A}|}$. Second, the results of the MAP decoder of the SF code are transformed from symbol to binary domain probabilities. Third, the binary domain results are deinterleaved. Fourth, the MAP decoder for the outer code decode with the deinterleaved binary probabilities. Fifth, the results of outer MAP decoder are interleaved and transformed to symbol domain probabilities. Sixth, we consider the symbol domain probabilities as the *a priori probability* for the inner MAP decode. This cycle is one decoding process. We decode iteratively with this cycle. We now describe each part of the decoding technique in detail. First, we consider the SISO MAP decoder for the SF (inner) code. The SISO MAP decoder calculates the *a posterior probability* (APP) from the received signals $\mathbf{Y}$ with the channel response $\mathbf{H}$. We show how to calculate APP using the BCJR algorithm [9] as follows. From the received signal $\sum_{\nu=1}^{N_r} y_n^\nu(p)$ and the *a-priori probability* $P(\tilde{x}_n^\mu(p))$, the $\gamma_p^i(s_{p-1}^i, s_p^i)$ value is computed as follows:

$$\gamma_p^i(s_{p-1}^i, s_p^i) = P(\tilde{x}_n^\mu(p)) \times \frac{1}{\sqrt{2\pi\sigma^2}} \exp \{-\frac{1}{2\sigma^2} |d_{free}(n,p)|^2\} \tag{12}$$

where σ^2 is the variance of AWGN and $d_{free}(n,p)$ is defined as

$$d_{free}(n,p) = \sum_{\nu=1}^{N_r} y_n^\nu(p) - \sum_{\nu=1}^{N_r} \sum_{\mu=1}^{N_t} H_{\mu\nu}^n \tilde{x}_n^\mu(p) \tag{13}$$

$\tilde{x}_n^\mu(p)$ shows the estimated symbol at the μth transmit antenna, pth subcarrier and nth symbol. Utilizing $\gamma_p^i(s_{p-1}^i, s_p^i)$, we calculate the values of $\alpha_p^i(s_p^i)$ and $\beta_{p-1}^i(s_{p-1}^i)$. For the sake of space limited, we omit the way to culculate $\alpha_p^i(s_p^i)$ and $\beta_{p-1}^i(s_{p-1}^i)$. The APP are

computed as follows:

$$\Pr(\tilde{S}_n(p) = a) = \sum_{\tilde{S}_n(p)=a} \gamma_p^i(s_{p-1}^i, s_p^i)\alpha_{p-1}^i(s_{p-1}^i)\beta_p^i(s_p^i). \quad (14)$$

a shows the symbol index, e.g. a is chosen from the symbol index $[0, 1, 2, 3]$ in the case of QPSK modulation. S_p^i shows the trellis state index of the inner code at the pth time slot. The results of the SISO MAP decoder of SF code are transformed to binary probability from the symbol domain probability as $\Pr(\tilde{b}'_c)$. The results which are transformed to binary probabilities are deinterleaved as follows:

$$\pi^{-1} : \Pr(\tilde{b}'_c) \rightarrow \Pr(\tilde{b}_c). \quad (15)$$

The deinterleaved binary probabilities are then considered as the inputs to the SISO MAP decoder of the outer (channel) code. The *a priori probability* of the outer code are constant values ($\frac{1}{2}$). We show how to calculate the LLR of the outer code as follows:

$$\gamma_k^o(s_{k-1}^o, s_k^o) = \frac{1}{2}\Pr(s_{k-1}^o, \Pr(b_c(k,p))|, s_k^o) \quad (16)$$

$$\Lambda(b_i(k,p)|\Pr(b_c(k,p))) = \ln\frac{\Pr(b_i(k,p)=+1)}{\Pr(b_i(k,p)=0)}$$

$$\Lambda(b_c(k,p)|\Pr(b_c(k,p))) = \ln\frac{\Pr(b_c(k,p)=+1)}{\Pr(b_c(k,p)=0)} \quad (17)$$

$b_i(k,p)$ and $b_c(k,p)$ show the information and coded data at the pth subcarrier and kth symbol interval. Λ shows the LLR of the outer code. We subtract only the channel value from Λ. The results of the subtraction are interleaved. The interleaved results are transformed to symbol domain probabilities ($P(\tilde{x}_n^\mu(p))$). The symbol domain probabilities are considered as the *a priori probability* for the inner code (SF code). Using this calculated *a priori probability* of the inner codes, we decode the signals once more. If the number of iterations is less than a maximum number allowed, we compare the APP of the outer code with zero.

4. Evaluations

In this section, we evaluate the proposed system. Consider that the channel model in this evaluation is a time-varying and frequency-selective Rayleigh fading channel where the center frequency is $1GHz$, the bandwidth is $1MHz$ and one OFDM frame consists of 128 sub-carriers and 100 symbols. For the sake of simplicity, we assume that each path from each transmit antenna to each receive antenna is independent and the channel gain is constant for one symbol and one subcarrier interval. Consider the case of a 2-transmit, 1-receive antenna and QPSK transmission system. We evaluate the BER performance with computer simulations.

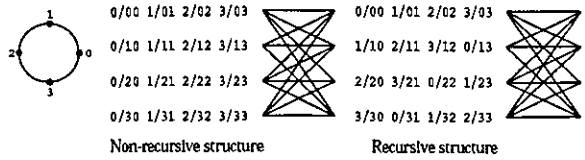

Figure 5: Trellis diagram for 2-transmit 4-state QPSK non-recursive/recursive space-frequency code.

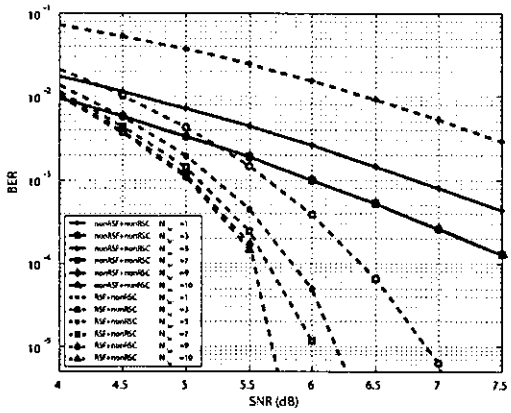

Figure 6: BER performance in the cases that the inner encoder is of recursive or non-recursive type.

4.1. Evaluation of the inner code

In this subsection, we evaluate the inner code. Fig. 5 shows the non-recursive [4] and recursive [5] 4-state QPSK 2 transmit space-frequency trellis diagrams. Fig. 6 shows the comparison between the case that the inner encoder is a non-recursive space-frequency (non-RSF) code and the case where it is a recursive space-frequency (RSF) code. The kind of interleaver is a random interleaver. In both cases, we use the 7-5 non-recursive systematic convolutional (non-RSC) code ($R_{ch} = 1/2$) as an outer code and the channel model is the time-varying and frequency-selective channel with the Doppler frequency $100Hz$ and delay spread $1\mu sec$. From fig. 6, it is seen that the better structure for inner encoder is of recursive type. N_{iter} shows the number of iterations. The performance of the concatenation between non-RSF and non-RSC codes can not

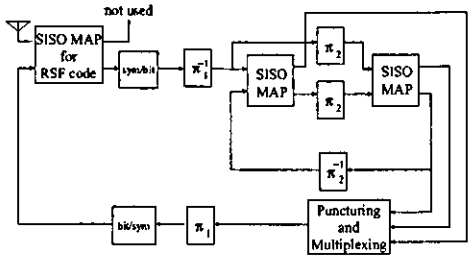

Figure 7: Decoding structure in the case that the outer code is a turbo code.

obtain an interleaver gain. From [8], in contrast with the case of a non-recursive inner encoder, the use of a recursive inner encoder yields an interleaver gain. As a consequence, the inner encoder must be a recursive encoder. The performance of the concatenation between the RSF and non-RSC codes converges at about 10 iterations. Hereinafter, we use the RSF code as an inner code and evaluate the systems using 9 iterations.

4.2. Evaluation of the outer code

In this subsection, we evaluate the outer code. Consider that the inner code is the RSF code and the interleaver between each code is a random interleaver. We evaluate three cases, first, the outer code is a 7-5 non-RSC code ($R_{ch} = 1/2$), second, the outer code is a 7-5 recursive systematic convolutional (RSC) code ($R_{ch} = 1/2$), and third, the outer code is a turbo code ($R_{ch} = 1/2$) which is punctured and consists of two 7-5 RSC codes ($R = 1/2$) and a random interleaver. Fig. 7 shows the decoder structure in the case that the outer code is a turbo code. π_1 shows the interleaver function for concatenation between inner and outer codes. π_2 show the interleaver function for the outer turbo code. In the decoding process of concatenation between RSF and turbo codes, we have the iterative decoding techniques of the time-frequency domain turbo code and the concatenation between the RSF (inner) code and turbo (outer) codes. We briefly explain the decoding process of the concatenation between the RSF (inner) code and turbo (outer) codes. The inner decoder computes the LLRs from the received signals. The results of inner decoding are deinterleaved and are considered as the inputs of the outer decoder. The outer decoder of the TF domain turbo code computes the LLRs with several iterations. After several iterative decodings of the turbo (outer) code, the results are interleaved and go to the inner decoder as the *a priori probability*. In one decoding cycle, there are the MAP decodings of inner code and the turbo decodings of outer code.

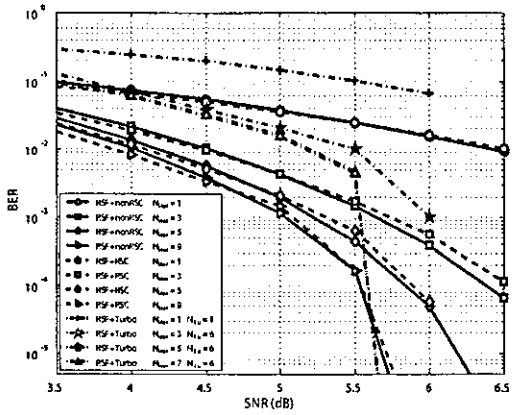

Figure 8: BER performance in the cases that the outer code is the non-RSC, RSC and trubo codes.

The computational complexity of the concatenation between RSF and turbo codes is much higher than that of the concatenation between RSF and non-RSC (or RSC) codes. We describe the computational complexity in section 5.

Fig. 8 shows the comparison between three cases where the Doppler frequency is $100Hz$ and the delay spread is $1\mu sec$. N_{Tu} shows the number of iterations for the turbo (outer) code. For the sake of high computational complexity, we consider that the maximum number of N_{Tu} and N_{iter} are 6 and 7 times respectively in the case that the outer code is turbo code. The concatenation between RSF and turbo codes has the best performance. However, the concatenation between RSF and turbo codes has much higher computational complexity than other two concatenated codes. The performance of the concatenation between RSF and turbo codes has a dominant effect over no concatenation between RSF (space-frequency domain) and turbo (time-frequency domain) codes but time-frequency domain turbo code. On the other hand, the performances of the concatenation between RSF and nonRSC/RSC codes have a dominant effect over concatenation between SF domain and TF domain codes. Comparison of nonRSC and RSC cases, it shows that better performance is obtained with nonRSC. In order to obtain more diversity gain over STF domain and interleaver gain between SF and TF codes, we interleave the encoded signals before transmitting. We assume that this interleaver is ideal. Therefore, we can consider that the channel response of each signal and each carrier is independent. Fig. 9 shows the BER performances in the case that the outer code is non-RSC and turbo codes where the channel response of each symbol and carrier

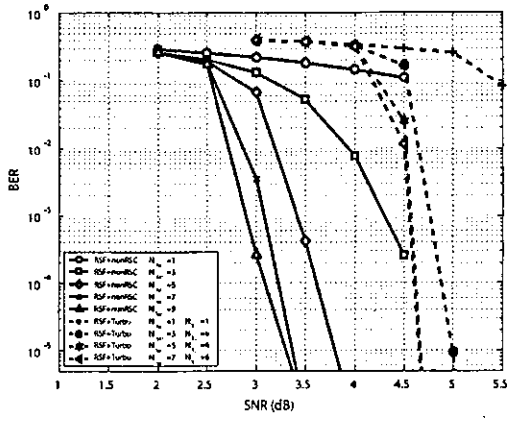

Figure 9: BER performance in the cases that the outer code is a RSC and non-RSC and turbo code and that the inner code is a recursive space-frequency code.

is independent. It is seen from fig. 9 that the concatenation between RSF and non-RSC codes has better performance than the concatenation between RSF and turbo codes. If we can obtain complete diversity and interleaver gains between SF and TF domain codes, the best structure of outer code is of non-RSC type. The best structure of an outer code is of non-recursive code which has a large Euclidean distance.

5. Computational Complexity

In this section, we describe the computational complexity. The computational complexity depends mainly on the number of states and paths from each state. Therefore, we count the number of all paths from each state during decoding one OFDM frame. Consider that the number of states of the outer/inner code is St_o/St_i, the number of paths from each state in the case of the outer/inner code is Pa_o/Pa_i and that the number of iterations is N_{iter}. In the case that the outer code is a RSC or non-RSC code and the inner code is a recursive or non-recursive space-frequency code, the computational complexity can be expressed as

$$\begin{aligned} C_c &= \{(Pa_o \times St_o) \times N_c \times (N_s \times \log_2 |\mathcal{A}_X|) \\ &+ (Pa_i \times St_i) \times N_c \times N_s\} \times N_{iter}. \end{aligned} \quad (18)$$

We assign $Pa_o = 2, Pa_i = |\mathcal{A}_X|$ to equation (18), and it can be rewritten as

$$\begin{aligned} C_c &= (2St_oN_cN_s \log_2 |\mathcal{A}_X| + |\mathcal{A}_X|St_iN_cN_s) \times N_{iter} \\ &= N_cN_sN_{iter}(2St_o \log_2 |\mathcal{A}_X| + |\mathcal{A}_X|St_i). \end{aligned} \quad (19)$$

In the case that the outer code is a turbo code and the inner is a recursive or non-recursive space-frequency code, we define the number of iterations of the outer code (when the turbo code consists of two element encoders with St_o states) as N_{Tu}. The computational complexity can be expressed as

$$\begin{aligned} C_t &= [\{2(Pa_o \times St_o) \times N_c \times (N_s \log_2 |\mathcal{A}_X|)\} \times N_{Tu} \\ &+ (Pa_i \times St_i)N_cN_s] \times N_{iter}. \end{aligned} \quad (20)$$

We assign $Pa_o = 2, Pa_i = |\mathcal{A}_X|$ to equation (20), therefore, it can be rewritten as

$$C_t = N_cN_sN_{iter}(4St_oN_{Tu} \log_2 |\mathcal{A}_X| + |\mathcal{A}_X|St_i). \quad (21)$$

In the case that we ignore the interleaver and deinterleaver function in the turbo (outer) code, the computational complexity of the concatenation between a RSF and a turbo codes is C_t/C_c times higher than the one between a RSF and non-RSC codes.

6. Conclusion

This paper proposed and investigated a serial concatenated code over STF domain. The proposed serial concatenated code can achieve high coding gain (interleaver gain) and diversity gain in the STF domain due to concatenation between different domain. The best structure of serial concatenation between different domain codes is that the type of outer encoder is non-recursive and the type of inner encoder is recursive.

References

[1] G. F. Foschini, Bell Labs. Tech. J., vol. q, no. 2, pp. 41-59, 1996.

[2] H. Sampath, et al., IEEE Trans. Commun., vol. 49, no. 12, pp. 2198-2206, Dec. 2001.

[3] K. Miyashita, et al, Proc. VTC2002-Fall, pp. 1302-1306, Sept. 2002

[4] V. Tarokh, et al., IEEE Trans. Inf. Theory, vol. 44, no. 2, pp. 744-765, Mar.1998.

[5] D. Tujkovic, Proc. Global Telecomm. Conf., vol. 2, Nov. 2000, pp.1010-1015.

[6] S. Zhou, et al., IEEE Signal Proc. Letters, Vol. 8, No.10, Oct. 2001

[7] Z. Liu, Y. Xin, et al., IEEE Trans. on Sig., vol. 50, no. 10, pp2465-2476, Oct. 2002.

[8] S. Benedetto, et al., IEEE Trans. Inf. Theory, vol.44, no.3, May 1998.

[9] L. R. Bahl, et al., IEEE Trans. Inf. Theory, pp. 284-287, July 1974.